Bachelor Thesis

Bachelor Mathematics

Spatiotemporal Dynamics of Cellular Cytokinesis

by

James Zoryk

July 1, 2023

Supervisor: prof.dr. Daniele Avitabile

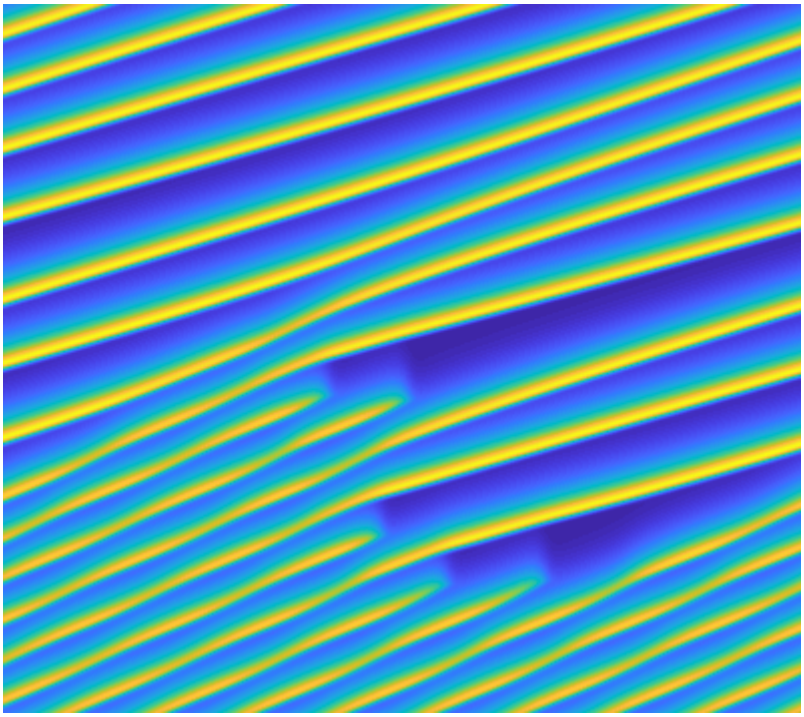

Department of Mathematics
Faculty of Sciences

VU UNIVERSITY AMSTERDAM

Abstract

The presence of travelling waves on the surface of starfish oocytes and other cellular systems during cytokinesis has sparked interest in understanding their precise dynamics [7]. This study aims to address this knowledge gap by investigating the behaviour of a reaction-diffusion model and exploring its parameter space to reveal bifurcation points and the emergence of travelling waves by numerical methods. The findings have the potential to enhance our understanding of cortical excitability and provide valuable insights into the self-organising patterns and dynamic behaviour exhibited by cells.

In this study, we employ a reaction-diffusion model to simulate the spatiotemporal dynamics of the cell cortex during cytokinesis. By varying the model parameters, we systematically explore the parameter space to identify regions where travelling waves arise. The numerical methods utilised allow for the efficient computation and visualisation of the evolving wave patterns.

Title: Spatiotemporal Dynamics of Cellular Cytokinesis
Author: James Zoryk, j.zoryk@student.vu.nl, 2663347
Supervisor: prof.dr. Daniele Avitabile
Date: July 1, 2023

Department of Mathematics
VU University Amsterdam
de Boelelaan 1081, 1081 HV Amsterdam
`http://www.math.vu.nl/`

Contents

1. General Introduction

The cell cortex, a dynamic region just beneath the plasma membrane, plays a crucial role in interpreting and responding to various intra- and extracellular signals, resulting in localised changes in cell shape and behaviour. One fascinating phenomenon observed in cellular systems is the emergence of dynamic patterns on the cell surface, including the presence of travelling waves. These patterns have been observed, for instance, on the surface of starfish oocytes, where they have been found to be associated with cortical excitability. However, despite their prevalence, the precise dynamics and underlying mechanisms of these travelling waves remain poorly understood.

In recent studies [7], researchers have investigated the cortical excitability observed during cytokinesis in both frog and starfish embryos. During this process, the cortical response to signals from the mitotic spindle leads to the assembly of an equatorial array of F-actin and myosin-2 known as the cytokinetic apparatus. This assembly drives an ingressing constriction, enabling cell division. Remarkably, these studies have revealed the existence of complementary waves of active Rho and F-actin that are focused and amplified at the equatorial cortex by the mitotic spindle. The dynamics of these waves exhibit features of travelling waves, which propagate across the cell surface. However, the underlying control networks and the specific nature of these travelling waves remain to be fully elucidated.

Understanding the mechanisms governing these travelling waves and their bifurcation diagram is a significant challenge in cell biology. To address this, the present study aims to investigate the spatiotemporal dynamics of the reaction-diffusion model [7],

$$\begin{cases} \partial_t u = d_u \Delta u + R(u, v, f(\alpha, \beta)) \\ \partial_t v = d_v \Delta v + R(u, v, f(\alpha, \beta)) - k_5 - k_6 v \\ \partial_t w = d_w \Delta u + k_7 + k_8 \frac{u^2}{1+k_9 u^2} - k_{10} w, \end{cases} \tag{1.1}$$

with

$$R(\cdot) = v \left(k_0 + \alpha \frac{k_1 u^3}{1 + k_2 u^2} \right) - u(k_3 + k_4 \, (1 + \beta) F) \, ,$$

which simulates the behaviour of the cortical excitability observed during cytokinesis. Through numerical simulations, we explore the parameter space of the model, with a particular focus on the group of proteins RGA-3/4 denoted as the β parameter. The β parameter represents a key factor influencing the behaviour of the system. By analysing the model's bifurcation diagram, we aim to uncover the critical points at which qualitative changes in the system's dynamics occur.

Furthermore, the study aims to demonstrate the existence of travelling waves in the model system. By tracking the behaviour of the main travelling wave branch through multiple simulations, we can observe the stages of wave formation, stability, and transition. These findings provide valuable insights into the spatio-temporal behaviour of the reaction-diffusion system and shed light on the occurrence of bifurcations and travelling waves in the context of cortical excitability.

2. Preliminaries Non-linear Dynamical Systems

In this chapter, we explore the fundamentals of non-linear dynamical systems, for a more detailed read see [14] . We start by revisiting the key properties of dynamical systems. The most basic continuous dynamical system is represented by a first-order ordinary differential equation (ODE) in two variables, denoted as $u(x,t)$:

$$\frac{d}{dt}u = u' = f(u,t), \tag{2.1}$$

where $f(u)$ is a continuous function. The variable $u(x,t)$ corresponds to the system's position within a two-dimensional space-time domain $\Omega \times \mathbb{R}_+$. This formulation captures the dynamic evolution of a system, describing how its state changes over time. Non-linear dynamical systems exhibit complex behaviour that cannot be easily predicted due to the absence of a linear relationship between inputs and outputs. In the subsequent sections, we will delve into the characteristics of non-linear systems, focusing on stability analysis and its linearisation. Additionally, we will discuss the significance of fixed points and their stability in understanding the behaviour of these systems.

2.1. Non-linear Systems

In order to discuss non-linear systems, it is essential to revisit the concept of linear systems.

Definition 2.1 (Linear System)**.** A well defined function $f(x)$ is a linear system if for scalars $a, b \in \mathbb{R}$ and $x, y \in \Omega$

$$f(ax + by) = af(x) + bf(x).$$

In simple terms, a linear system is characterised by the property that its output is directly proportional to its input, as expressed by the superposition principle. However, non-linear systems do not exhibit this proportionality, making it challenging to predict the system's output given a change in input. Generally, solving non-linear systems is significantly more difficult than solving linear systems, often requiring numerical methods as closed-form solutions are not always possible. Nonetheless, the dynamics of non-linear systems can still be analysed through linear stability and bifurcation theory. These approaches provide insights into the behaviour and qualitative properties of non-linear systems, despite the absence of exact solutions.

2.2. Linear Stability Analysis

Fixed points, where the dynamics of a system become stationary over time, play a crucial role in stability analysis. A state u^* is considered a fixed point of Eq.(2.1) if it remains unchanged under the given dynamics.

Definition 2.2 (Fixed Point)**.** Given the dynamical system Eq.(2.1), then u^* is a fixed point of the system if $f(u^*) = 0$.

When studying fixed points, an important question arises regarding their stability, as they can be either stable or unstable. To assess the stability of a fixed point, we examine small

perturbations around it. For a stable fixed point, the perturbation will decrease over time, eventually converging back to the original fixed point.

First we shall introduce an important theorem that we will use through this paper which is called Taylor's Theorem:

Theorem 2.3 (Taylor's Theorem)**.** *If a function $f(x)$ has a continuous derivatives up to the $(n+1)$th order on a closed interval containing the point x_0 and x_0+h for some $h>0\in\mathbb{R}$, then*

$$f(x_0+h)=f(x_0)+hf'(x_0)+\ldots+\frac{h^n}{n!}f^{(n)}(x_0)+\mathcal{O}(h^{n+1}).$$

To analyse the stability, let us consider a small perturbation $\tilde{u}$ around the fixed point u. We express u as $u=u^*+\tilde{u}$, with $|\tilde{u}|\ll 1$, for the dynamical system in Eq.2.1. By applying Taylor's Theorem 2.3, we have:

$$\begin{aligned}u' &= u^{*\prime}+\tilde{u}'\\ &= f(u^*+\tilde{u},t)\\ &= f(u^*,t)+f'(u^*,t)\tilde{u}+\mathcal{O}(\tilde{u}^2),\end{aligned}$$

then since u^* is a fixed point by definition 2.2, the term $f(u^*,t)=0$. Hence we are left with

$$\tilde{u}'=f'(u^*,t)\tilde{u}.$$

In this linearised form around the fixed point u^*, the higher order terms $\mathcal{O}(\tilde{u}^2)$ are neglected, giving rise to the name "linear stability analysis." For dynamical systems with more than one equation, $f'(\cdot)$ represents the Jacobian matrix evaluated at the fixed point:

$$f'(\boldsymbol{u}^*,t)=J^*=\frac{\partial f_i}{\partial u_i}\Big|_{\boldsymbol{u}^*}.$$

Furthermore, we assume that we can expressed the perturbation as $\tilde{\boldsymbol{u}}=\boldsymbol{\varphi}e^{\lambda_i t}$, we can construct the following eigenvalue problem

$$\lambda_i\boldsymbol{\varphi}=J^*\boldsymbol{\varphi} \tag{2.2}$$

with λ_i being the eigenvalue and $\boldsymbol{\varphi}$ denoting the eigenfunctions. Since λ can be complex we can then write the expression as

$$e^{\lambda_i t}=e^{\mathrm{Re}(\lambda_i)t}e^{\mathrm{Im}(\lambda_i)t}.$$

Therefore we can conclude that a fixed point is stable if all eigenvalues are negative, while the fixed point is unstable if the eigenvalues are positive.

Theorem 2.4 (Stable Fixed point)**.** *If u^* is a fixed point of the system Eq.(2.1) with λ_i the eigenvalues of the eigenproblem Eq.(2.2), then u^* is stable if* $\mathrm{Re}(\lambda_i)<0\ ,\forall i$.

Theorem 2.5 (Unstable Fixed point)**.** *If u^* is a fixed point of the system Eq.(2.1) with λ_i the eigenvalues of the eigenproblem Eq.(2.2), then u^* is unstable if $\exists i$ s.t* $\mathrm{Re}(\lambda_i)>0$.

However, if it is the case that $\mathrm{Re}(\lambda)=0$ then we class this as a neutral stability, which implies that we can not conclude the stability from the linear stability analysis.

3. Reaction-Diffusion Theory

One fascinating aspect of natural phenomena is the formation of spatial or spatiotemporal patterns, often observed in various contexts such as animal coats, sand dune ripples, and vegetation growth in semi-arid conditions [4, 13, 15]. These patterns exhibit recognisable structures that are not random but possess a certain periodicity or regularity, often in the form of stripes or spots [8, 3]. Understanding the underlying mechanisms behind the formation of these patterns has been a subject of interest in fields ranging from biology to chemistry.

One of the notable systems where spatial patterns emerge is in chemical systems described by reaction-diffusion processes. The Belousov-Zhabotinsky reaction, for instance, involves the oxidation of malonic acid by bromate ions in the presence of ferroin catalysts, which exhibits distinct spatial patterns [5]. In this paper, we will explore the linear stability analysis of the simplest reaction-diffusion system that gives rise to pattern formation from a uniform state, following the work of Turing in his seminal 1952 paper [2]. Through this analysis, we aim to gain insights into the mechanisms of pattern formation in reaction-diffusion systems.

Our investigation will lead us to several key findings, some of which were unexpected at the time:

i. At least two interacting chemicals are necessary for pattern formation to occur in the system.

ii. Turing's most surprising insight was that diffusion in the chemical system can actually be a destabilising influence, leading to instability in certain cases.

iii. The instability caused by diffusion can result in the growth of structures at specific wavelengths, dependent on the system.

iv. Pattern formation in a chemical system requires a significant difference in the diffusion coefficients of the involved chemicals. This realisation was not immediately apparent and took several years for experimental confirmation after Turing's initial theory.

3.1. Reaction-Diffusion Equations

The reaction-diffusion equations are partial differential equations that can be written in the following form:

$$\frac{\partial \mathbf{u}}{\partial t} = \mathbf{D}\Delta\mathbf{u} + \mathbf{R}(\mathbf{u}, p), \tag{3.1}$$

where $\mathbf{u} = (u_1(x,t), u_2(x,t), \ldots, u_n(x,t))$ represents the concentrations of n chemical species at position x and time t. Here, x belongs to the spatial domain $\Omega := [-L, L]$ and t belongs to the nonnegative real numbers $\mathbb{R}+$. The term $\mathbf{D}\Delta\mathbf{u}$ represents the diffusion term, where $\mathbf{D}$ is a diagonal matrix of diffusion coefficients:

$$\mathbf{D} = \begin{pmatrix} 1 & 0 & \ldots & 0 \\ 0 & d_1 & \ldots & 0 \\ \vdots & \vdots & \ddots & \vdots \\ 0 & 0 & \ldots & d_n \end{pmatrix} \tag{3.2}$$

Here, $d_1, d_2, \ldots, d_n$ are the diffusion coefficients. The first element of $\mathbf{D}$ is set to 1 to non-dimensionalise the system. The operator Δ denotes the Laplacian operator, which in one-dimensional spatial coordinates x takes the form:

$$\Delta = \frac{d^2}{dx^2}. \tag{3.3}$$

The term $\mathbf{R}(\mathbf{u}, p)$ represents the sum of the reaction kinetics for each chemical species, given by $r_1(\mathbf{u}, p), r_2(\mathbf{u}, p), \ldots, r_n(\mathbf{u}, p)$. Here, p denotes the parameters involved in the reaction kinetics.

3.1.1. Diffusion

Diffusion is a fundamental mechanism that models the thermal motion of particles in chemical systems. It is responsible for the transport of particles from regions of high concentration to regions of lower concentration. This transport occurs due to the random motion and collisions of particles in a fluid, such as a liquid or gas. Each particle undergoes constant random thermal motion, which occurs on very small length scales and is not observable to the naked eye. The random movements of individual particles are not correlated, preventing bulk movement of the fluid. Therefore, diffusion can take place in both still and moving fluids.

Diffusion is often associated with Brownian motion, which refers to the random motion of an individual particle. However, diffusion itself describes the behaviour of an ensemble of particles. A well-known example of diffusion is the dispersion of a small amount of smoke released in a still room, where the smoke particles disperse and spread out over time.

From a mathematical perspective, diffusion is described by partial differential equations. These equations capture the spread of particles through the process of diffusion. For a detailed mathematical explanation of diffusion, we refer the reader to [9].

It may initially seem paradoxical that diffusion, which tends to homogenise concentrations and make particle distributions more uniform, can lead to pattern formation. Patterns, by definition, require particles of the same type to clump together and form coherent spatial structures. However, through the interplay of diffusion with other factors, such as reaction kinetics, spatial heterogeneity, and non-linear dynamics, diffusion can give rise to complex patterns and structures in chemical systems. Understanding how diffusion contributes to pattern formation is a central focus of reaction-diffusion theory.

3.1.2. Boundary Conditions

When solving partial differential equations, including reaction-diffusion systems, it is necessary to define both the initial conditions and the boundary conditions of the domain.

The initial conditions specify the concentrations of the chemical species at the beginning of the simulation, typically at time $t = 0$. These initial concentrations serve as the starting point for the system's evolution over time. In addition to the initial conditions, boundary conditions are required to model the behaviour of the system at the boundaries of the domain. Boundary conditions define how the concentrations of the chemical species are constrained or influenced at the edges of the system. The choice of boundary conditions depends on the specific physical conditions being modelled. For example, in the case of cells, the cell membrane acts as a barrier that prevents the exchange of particles of interest. In this case, no-flux boundary conditions, also known as Neumann boundary conditions, are often used. These conditions enforce that the flux of particles across the boundary is zero.

In the examples examined in this paper, we consider the membrane of a cell, which is assumed to be spherical. In mathematical terms, this corresponds to periodic boundary conditions, where the concentrations at one edge of the domain are equal to the concentrations at the opposite edge. Mathematically, this can be expressed as:

$$u(-L, t) = u(L, t) \quad \text{and} \quad \frac{du}{dx}(-L, t) = \frac{du}{dx}(L, t) \quad \forall t \in \mathbb{R}_+. \tag{3.4}$$

For the examples presented in this paper, we will consider periodic boundary conditions. These conditions allow for the formation of periodic patterns and are particularly relevant when studying systems with spatial periodicity.

3.2. Turing Patterns

Turing patterns are spatial patterns that emerge in reaction-diffusion systems. In this section, we will discuss the conceptual framework of general linear analysis to gain a better understanding of the mechanics behind Turing patterns.

We consider a domain Ω with periodic boundary conditions. Recall condition (ii) mentioned in the introduction of this chapter, which states that in the absence of diffusion, the state is stable in a base solution $\boldsymbol{u}^*$, meaning that $\boldsymbol{R}(\boldsymbol{u}^*, p^*)$ for some control parameter p^* and $\boldsymbol{J}^*$ has negative eigenvalues (according to Theorem 2.4).

To determine the stability of a fixed point, we consider a small perturbation around the fixed point. We assume that the perturbation is small compared to the fixed point itself:

$$\boldsymbol{u}(x,t) = \boldsymbol{u}^* + \tilde{\boldsymbol{u}}, \quad |\tilde{\boldsymbol{u}}| << 1. \tag{3.5}$$

Linearising Equation 3.1 around the fixed point $\boldsymbol{u}$ using Taylor's Theorem 2.3, we obtain the expression:

$$\partial_t \tilde{\boldsymbol{u}} = \boldsymbol{J}^+ \boldsymbol{D} \Delta \tilde{\boldsymbol{u}}, \tag{3.6}$$

where $\boldsymbol{J}$ represents the Jacobian matrix of $\boldsymbol{R}$ and Δ is the Laplacian operator. By assuming a perturbation of the form:

$$\tilde{\boldsymbol{u}} = c \exp\left[\lambda_j t + ikx\right],$$

for some constant c, and taking the second-order derivative of the perturbation, we arrive at the eigenproblem:

$$\left|\lambda \boldsymbol{I} - \boldsymbol{J}^* + k^2 \boldsymbol{D}\right| = 0, \tag{3.7}$$

where k is the non-dimensional wave number associated with the spatial pattern, λ represents the eigenvalue, and $\boldsymbol{I}$ is the identity matrix.

The characteristic equation given by Equation 3.7 determines the eigenvalues λ_j that govern the stability of the system. Under specific conditions, the diffusion coefficients $\boldsymbol{D}$ can cause a stable state to become unstable, leading to the formation of Turing patterns. By solving the characteristic equation, we can analyse the stability and determine the conditions under which Turing patterns can arise.

3.2.1. General case for two chemical systems

In order to investigate the conditions for the occurrence of Turing patterns in a reaction-diffusion system with two chemicals, let's consider the following equations:

$$\begin{cases} \partial_t u &= \partial_{xx} u + f(u,v,p), \\ \partial_t v &= \partial_{xx} v + g(u,v,p). \end{cases} \tag{3.8}$$

In the absence of diffusion, the system can be represented by the following set of ordinary differential equations:

$$\dot{u} = f(u,v,p), \qquad \text{and} \qquad \dot{v} = g(u,v,p)$$

where $\dot{u}$ and $\dot{v}$ represent the time derivatives of u and v respectively. Assuming that the system has a steady state $\boldsymbol{u}^* = (u^*, v^*)$ for some parameter p^*, we can linearise the system around this fixed point using the Jacobian matrix $\boldsymbol{J}^*$:

$$\boldsymbol{J}^* = \begin{pmatrix} f_u & f_v \\ g_u & g_v \end{pmatrix} \Bigg|_{\boldsymbol{u}^*}$$

The determinant and trace of $\boldsymbol{J}^*$ can be computed as:

$$\begin{aligned} \operatorname{tr}(\boldsymbol{J}^*) &= f_u + g_v \\ \det(\boldsymbol{J}^*) &= f_u g_v - f_v g_u, \end{aligned}$$

By constructing the characteristic equation for the eigenproblem, we obtain:

$$\lambda^2 - \lambda \operatorname{tr}(\boldsymbol{J}^*) + \det(\boldsymbol{J}^*) = 0, \tag{3.9}$$

The eigenvalues of the system are given by:

$$\lambda_\pm = \frac{1}{2}\left(\operatorname{tr}(\boldsymbol{J}^* \pm \sqrt{\operatorname{tr}(\boldsymbol{J}^{*2} - 4\det(\boldsymbol{J}^*)}\right).$$

For the steady state $\boldsymbol{u}^*$ to be stable, we require the following conditions to be satisfied:

$$\operatorname{tr}(\boldsymbol{J}^*) < 0, \qquad \text{and} \qquad \det(\boldsymbol{J}^*) > 0.$$

Now, considering the case when diffusion is present, we can extend the eigenproblem to:

$$\boldsymbol{D}\partial_{xx} + \boldsymbol{J}^*$$

where $\boldsymbol{D} = \operatorname{diag}(1, d)$ is the diffusion coefficient matrix. This yields the extended characteristic equation:

$$\lambda^2 + \lambda\alpha(k^2) + \beta(k^2) = 0, \tag{3.10}$$

here denoting the terms

$$\begin{aligned}\alpha(k^2) &= k^2(1+d) - (f_u + g_v),\\ \beta(k^2) &= dk^4 - (df_u = g_v)k^2 + \det(\boldsymbol{J}^*).\end{aligned}$$

The eigenvalues can be expressed as:

$$\lambda_{1,\,2}(k^2) = \frac{1}{2}\left(\alpha(k^2) \pm \sqrt{\alpha(k^2)^2 - 4\beta(k^2)}\right)$$

Since we assume $\operatorname{tr}(\boldsymbol{J}^*) < 0$, it implies that $\beta(k^2) < 0$ for some k. Therefore, we need the condition $df_u + g_v > 0$, which means that the diffusion coefficient d must be different from 1, and $f_u g_v < 0$ must hold.

In summary, we can formulate Lemma 3.1, the conditions for Turing instability in a system with two chemicals (described by Equations 3.8) are:

Lemma 3.1 (Turing-Instability)**.** *For a system with two chemicals as in Eq.(3.8) a Turing-Instability will occur if the following conditions are meet:*

i) $f_u + g_v < 0$.

ii) $f_u g_v - f_v g_u > 0$.

iii) $df_u + g_v > 0$.

iv) $df_u + g_u > 2\sqrt{d(f_u g_v - f_v g_u)}$.

4. Bifurcation Theory

Bifurcation theory studies the qualitative changes in the behaviour of dynamical systems as parameters are varied. Two important types of bifurcations are the Hopf bifurcation and the Turing bifurcation. In some cases, a system can exhibit both a Hopf bifurcation and a Turing bifurcation simultaneously, leading to a Turing-Hopf bifurcation. For this section we follow [12].

4.1. Hopf Bifurcation

A Hopf bifurcation occurs when a system undergoes a qualitative change in its stability, leading to the emergence of a periodic solution. It is a local bifurcation that occurs when a fixed point of a dynamical system loses stability as a pair of complex conjugate eigenvalues of its linearisation cross the imaginary axis. The conditions for a Hopf bifurcation of the homogeneous steady state are as follows:

Lemma 4.1 (Hopf Bifurcation)**.** *For a reaction-diffusion system define as Eq.(3.1), at wave number $k = 0$ a and some parameter p^*, a Hopf-Bifurcation will occur if*

$$\mathrm{Re}\left[\lambda_j(p^*, 0)\right] = 0, \quad \textit{and} \quad \mathrm{Im}\left[\lambda_j(p^*, 0)\right] \neq 0.$$

At the Hopf bifurcation, the eigenvalues $\lambda_j(p_c, 0)$ become purely imaginary, i.e., $\lambda_j(p_c, 0) = \pm i\omega$ for some $\omega \in \mathbb{R}_{\neq 0}$. The steady state $\boldsymbol{u}^*$ becomes unstable to perturbations, and we expect the emerging solution to exhibit oscillations with a period of $T = 2\pi/\omega$. If the bifurcation is supercritical, we should observe homogeneous oscillations with a period of T.

4.2. Turing Bifurcation

A Turing bifurcation is a pattern-forming bifurcation that occurs when a homogeneous steady state becomes unstable, leading to the formation of spatial patterns. The conditions for a Turing bifurcation in a reaction-diffusion system are as follows:

Lemma 4.2 (Turing-Bifurcation)**.** *For a reaction-diffusion system defined as Eq.(3.1), then at a critical wave number $k_c \neq 0$ and some parameter p^* a Turing-Bifurcation will occur if*

$$\mathrm{Re}\left[\lambda_j(p^*, k_c)\right] = 0, \quad \textit{and} \quad \mathrm{Im}\left[\lambda_j(p^*, k_c)\right] = 0.$$

The Turing bifurcation leads to the formation of spatial patterns in the system, characterised by the interaction between diffusion and reaction processes.

4.3. Turing Hopf Bifurcation

In some cases, a system can exhibit both a Hopf bifurcation and a Turing bifurcation simultaneously, resulting in a Turing-Hopf bifurcation.

Lemma 4.3 (Turing-Hopf-Bifurcation)**.** *For a reaction-diffusion system defined as Eq.(3.1), then at a critical wave number $k_c \neq 0$ and some parameter p^* a Turing-Bifurcation will occur if*

$$\mathrm{Re}\left[\lambda_j(p^*, k_c)\right] = 0, \quad \textit{and} \quad \mathrm{Im}\left[\lambda_j(p^*, k_c)\right] \neq 0.$$

In the case of a Turing-Hopf bifurcation, both pattern formation and oscillatory behaviour are observed in the system. The emergence of spatial patterns and oscillations can have important implications in various fields, such as chemistry, biology, and physics.

5. Numerical Analysis

In many cases, the problems described in this paper cannot be solved analytically. Therefore, numerical methods on digital computers become essential tools. With the increasing performance of digital computers and the availability of modern algorithms, we can now quantitatively investigate the evolution equations that describe reaction-diffusion systems. Numerical simulations serve as a valuable third approach, complementing theoretical and experimental methods, to explore and understand the mechanisms of reaction-diffusion systems.

In this section, we will discuss the underlying assumptions of numerical methods used to study pattern-forming systems, providing insights into the reliability of simulations. We will introduce and discuss some numerical ideas and tools employed to solve problems in this field. Numerical investigations are akin to laboratory experiments, as they provide approximate answers to specific questions. By selecting parameter values, boundary conditions, initial states, and observing the system for a finite duration, we can gain understanding about the behaviour of specific solutions to the equations of interest. A numerical study often requires multiple repetitions with different parameter values spanning a range of interest. Even then, only an approximate understanding of the system's behaviour can be deduced. Analytical methods, in contrast, can often provide explicit mathematical predictions of how phenomena vary with parameters. However, analytical methods are not automatically superior to numerical or experimental approaches, as they rely on mathematical or physical assumptions whose range of validity may not be known beforehand. Progress in understanding pattern formation in reaction-diffusion systems necessitates a comparison of analytical results, numerical simulations, and experimental observations.

5.1. Finite Difference Method

The finite difference method is a technique that replaces the differential operator in a differential equation with a finite difference matrix, transforming it into a linear $\boldsymbol{A}x = \boldsymbol{b}$ type of expression. This method can be extended to replace the differential operator in partial differential equations, allowing us to approximate the PDE by a system of ordinary differential equations.

In the context of a one-dimensional domain Ω, we divide the space uniformly into a set of grid points denoted as $\{x_j\}_{j=1}^n$, where $x_j = jh$. Here, n represents the number of grid points, h denotes the grid spacing, and it is defined as

$$h = \frac{b-a}{n},$$

where a and b represent the bounds of the domain Ω. Consequently, the approximation to the solution u can be represented as a finite sequence $\{u_j\}_{j=0}^n$, defined only at the corresponding grid points. We note that u_j approximates the value of u at x_j, namely $u_j \approx u(x_j)$. To approximate the second derivative $u''(x_j)$, we replace it with the second-order centred finite difference expression obtained using the Taylor series expansion theorem 2.3:

$$\frac{u_{j+1} - 2u_j + u_{j-1}}{h^2} = f(x_j) \quad \text{for} \quad j = 1, 2, \dots n.$$

This equation corresponds to the discretisation of the differential equation using finite differences. By defining $\mathbf{u} = (u_1, u_2, \dots, u_n)^T$ and $\mathbf{u}'' = (u_1'', u_2'', \dots, u_n'')^T$, where $u_i'' = u''(x_i)$, we can express the system of equations as:

$$\boldsymbol{D}_{xx}\mathbf{u} \approx \mathbf{u}'', \tag{5.1}$$

where $\boldsymbol{D}_{xx}$ is a symmetric $n \times n$ finite difference matrix defined as:

$$\boldsymbol{D}_{xx} = \frac{1}{h^2}\,\text{tridiag}(-1, 2, -1) = \frac{1}{h^2}\begin{bmatrix} 2 & -1 & 0 & \dots & 0 \\ -1 & 2 & -1 & \dots & 0 \\ 0 & -1 & 2 & \ddots & 0 \\ \vdots & \vdots & \ddots & \ddots & -1 \\ 0 & 0 & \dots & -1 & 2 \end{bmatrix}.$$

This matrix represents the discrete operator for the second derivative in the finite difference scheme. Therefore, the reaction-diffusion system described by Eq. 3.8 can be discretised by choosing n grid points for the domain, allowing us to represent the functions u and v as follows:

$$\boldsymbol{u}(x,t) = \big(u_1(x,t),\, u_2(x,t),\, \dots u_n(x,t)\big)^T,$$
$$\boldsymbol{v}(x,t) = \big(v_1(x,t),\, v_2(x,t),\, \dots v_n(x,t)\big)^T.$$

Similarly, we define the reaction terms as:

$$\boldsymbol{f}(u,v,p) = \big(f_1(u,v,p),\, f_2(u,v,p),\, \dots\, f_n(u,v,p)\big)^T,$$
$$\boldsymbol{g}(u,v,p) = \big(g_1(u,v,p),\, g_2(u,v,p),\, \dots\, g_n(u,v,p)\big)^T.$$

To simplify the notation, let $\boldsymbol{z} = (\boldsymbol{u}, \boldsymbol{v})^T$ and $\boldsymbol{h} = (\boldsymbol{f}, \boldsymbol{g})^T$. We can represent the $n \times n$ differential matrix $\boldsymbol{D}xx$ and construct a $2n \times 2n$ matrix operator $\tilde{\boldsymbol{D}}xx$ by combining $\boldsymbol{D}xx$ with the corresponding diffusion coefficient:

$$\tilde{\boldsymbol{D}}_{xx} = \begin{pmatrix} \boldsymbol{D}_{xx} & 0 \\ 0 & d\boldsymbol{D}_{xx} \end{pmatrix}.$$

Hence, we have created a linear system for a two-chemical reaction-diffusion system:

$$\dot{\boldsymbol{z}} = \tilde{\boldsymbol{D}}_{xx}\boldsymbol{z} + \boldsymbol{h}(\boldsymbol{u}, \boldsymbol{v}, p). \tag{5.2}$$

5.2. Continuation Methods

Bifurcation analysis is a powerful tool for understanding the behavior of nonlinear systems. While analytical approaches have traditionally been used for studying bifurcations, numerical methods have emerged as valuable alternatives. In particular, continuation methods provide an effective means to explore bifurcations and track solution branches in a numerical framework.

Previously, we made the following assumptions and focused on bifurcations from a known base or fixed-point solution, performing weakly nonlinear local analysis around that solution.However, in general, we encounter broader scenarios where:

i. Obtaining the base solution: It is necessary to find a base solution. This involves solving the underlying equations under specific conditions to establish a starting point for further exploration.

ii. Exploring distant bifurcations: In addition to investigating bifurcations in close proximity, it is often crucial to understand the connections between bifurcations that are separated by a finite distance. These bifurcations cannot be connected via a higher singularity, making it necessary to explore solution branches that extend far away from the initial bifurcation points.

iii. Following solution branches: Numerical methods offer the flexibility to follow solution branches and navigate through bifurcations, even when they are located at a significant distance from the starting point. These methods allow us to systematically trace the behaviour of the system as parameters vary.

One specific numerical method commonly used for bifurcation analysis is arclength continuation. This approach involves incrementing an arc length parameter while tracing the solution branches. Continuation ensures smooth continuation along the branches by employing specialised algorithms that detect and characterise bifurcation points encountered along the way. This method enables us to compute solution points and determine their stability properties.

For a more detailed discussion of continuation methods, the reader can refer to [6] and a good introduction can be found in [1].

By embracing numerical methods, particularly continuation methods, we can overcome the limitations of analytical approaches. These numerical techniques empower us to explore solution branches, investigate bifurcations both near and far, and gain deeper insights into the dynamics of nonlinear systems.

6. Schnakenberg Model - Example

In order to illustrate the techniques and tools presented in this paper, we will examine them in the context of a simpler system that allows for analytical solutions and result comparisons. Our focus will be on the Schnakenberg system [11], which is a partial differential equation. By analysing this system, we will investigate its unique steady state and derive stability conditions through analytical solutions. The Schnakenberg system is particularly suitable for this purpose.

The Schnakenberg system consists of two equations governing the dynamics of the variables u and v, represented as:

$$\begin{cases} \partial_t u &= \Delta u + \eta r_1 \\ \partial_t v &= d\Delta v + \eta r_2. \end{cases} \tag{6.1}$$

Where we define the reaction terms for the parameter $\boldsymbol{p} = (\eta, a, b, d)$ as

$$\begin{cases} r_1(u, v, p) := a - u + u^2 v, \\ r_2(u, v, p) := b - u^2 v. \end{cases}$$

We consider the case for periodic boundary conditions. In this context, both species are uniformly generated throughout the domain. The variable u undergoes linear decay, while v undergoes non-linear and autocatalytic conversion to u. The diffusion rate d influences the relative speed of dispersal between the two species, and the parameter η determines the balance between diffusion and the chemical reaction.

6.1. Analytical Analysis.

In a one-dimensional domain with periodic boundary conditions, the spatially homogeneous steady state (HSS) solutions of the Schnakenberg system satisfy the following equations:

$$r_1(u, v, p) = 0, \quad \text{and} \quad r_2(u, v, p) = 0.$$

By solving these equations, we can determine the unique position of the HSS, denoted as $\boldsymbol{u}^* = (u^*, v^*)^T$, which is given by:

$$\boldsymbol{u}^* = \left(a + b \,,\, \frac{b}{(a+b)^2} \right)^T$$

Next we can linearise the Schnakenberg system as described by Eq.(3.6) to obtain the eigenproblem for the system, where

$$\boldsymbol{J} := \begin{pmatrix} -1 + 2uv & u^2 \\ -2uv & -u^2 \end{pmatrix}, \quad \text{and} \quad \boldsymbol{D} := \begin{pmatrix} 1 & 0 \\ 0 & d \end{pmatrix}.$$

By analysing the eigenvalues of the linear operator associated with the system, we can determine the stability of the HSS. Therefore we evaluate the Jacobian around the fixed point HSS, which is expressed as

$$\boldsymbol{J}^* = \begin{pmatrix} \frac{b-a}{a+b} & (a+b)^2 \\ \frac{-2b}{a+b} & -(a+b)^2. \end{pmatrix} = \begin{pmatrix} J_{11} & J_{12} \\ J_{21} & J_{22}. \end{pmatrix}$$

In order for a Turing instability to occur in the system, such that pattern will form, we need Lemma[3.1] to hold, thus for the Schnakenberg system we have:

i. $J_{11} + J_{22} < 0 \implies 0 < b - a < (a+b)^3$.

ii. $J_{11}J_{22} - J_{12}J_{21} > 0 \implies (a+b)^2 > 0$.

iii. $dJ_{11} + J_{22} > 0 \implies d(b-a) > (a+b)^2 > 0$.

iv. $dJ_{11} + J_{22} > 2\sqrt{d\,(J_{11}J_{22} - J_{12}J_{21})} \implies \left(d(b-a) - (a+b)^3\right)^2 > 4d(a+b)^3$.

Employing the assistance of the computer program Mathematica, to find parameters $\boldsymbol{p}$ that hold for the conditions stated above.

6.1.1. Hopf Bifurcation

In this section, we investigate the parameter values that satisfy the conditions of Lemma 4.1 for a Hopf steady state. We start with a simple case where $p_1^s = (1, 0.1, 0.74, 1)$, as shown in Figure [6.1]. The x-axis represents the wave number k, while the y-axis denotes the function values of both the real and imaginary parts of the two eigenvalues of the system. From the figure, we observe that $\lambda_1(0) > 0$ and the imaginary parts are non-zero, indicating a Hopf bifurcation.

Similarly, we analyse another interesting case for $p_2^s = (7, 0.15, 0.21, 20)$, depicted in Figure [6.2]. For p_2^s, we find a value of $k \approx \pm 0.75$ that is close to being above zero, which would satisfy the conditions of Lemma 4.2. However, we discover that p_2^s is actually a Hopf bifurcation point.

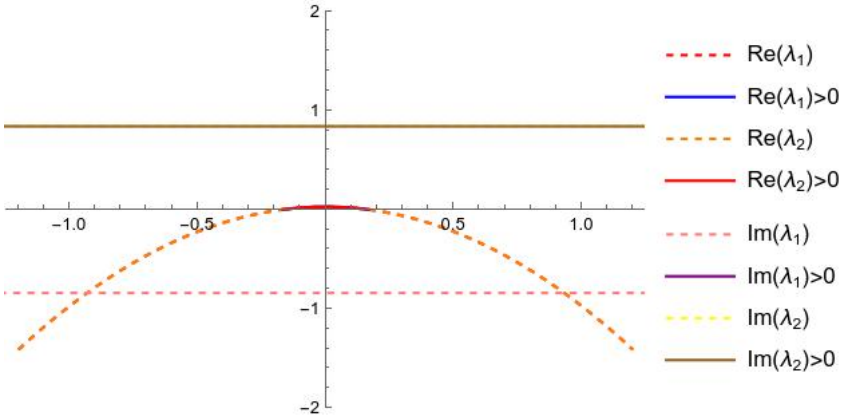

Figure 6.1.: Hopf bifurcation occurs for $p_1^s = (1, 0.1, 0.74, 1)$.

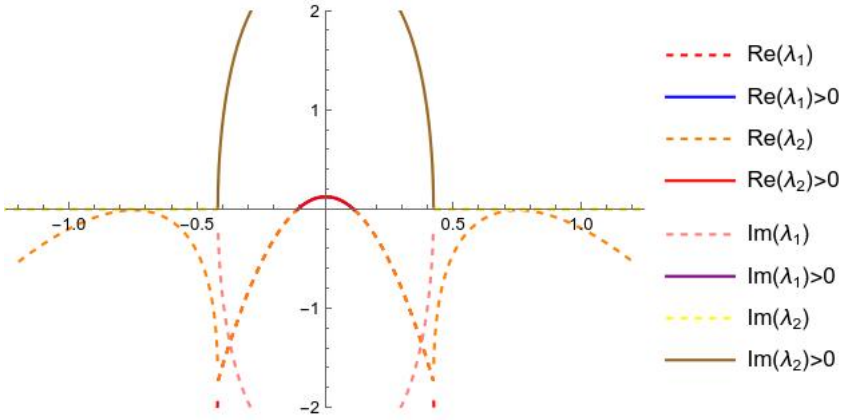

Figure 6.2.: Illustration for $p_2^s = (7, 0.15, 0.21, 20)$.

6.1.2. Turing Bifurcation

The Schnakenberg system also exhibits Turing bifurcation points. One such point is found at the parameter value $p_3^s = (7, 0.175, 0.21, 100)$. Figure [6.3] provides a visual plot illustrating this case. It is evident that p_3^s satisfies the conditions outlined in Lemma 4.2.

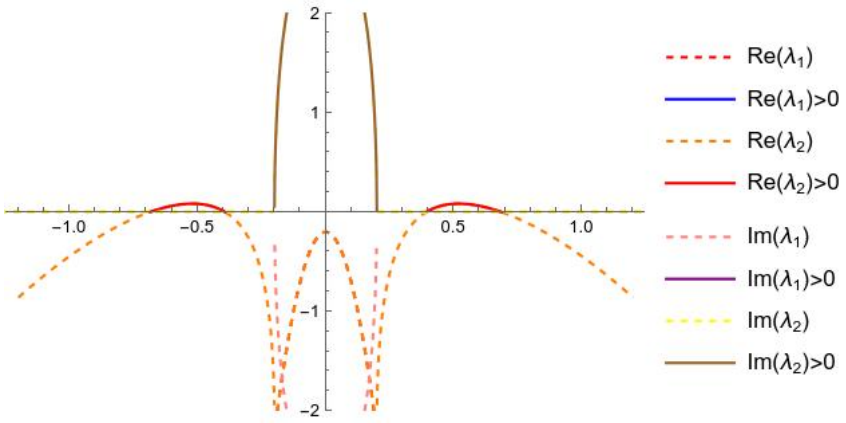

Figure 6.3.: Turing bifurcation occurs for $p_3^S = (7, 0.175, 0.21, 100)$.

6.2. Numerical Analysis

In order to validate the theoretical results presented in Chapter 5, we can implement them in MATLAB and compare the numerical results with the analytical solutions for the Schnakenberg system. This allows us to refine the software tools and methods and gain confidence in our numerical techniques before applying them to more complex scenarios in later chapters.

6.2.1. Time Stepping

To approximate the Schnakenberg system given by Eq.6.1 using finite differences, as described in Chapter 5, we discretise the domain into $n = 100$ points and apply the discrete matrix approximation for Δ (Eq. 5.1). We also discretise u and v as $\boldsymbol{u} = (u_1, u_2, \ldots, u_n)^T$ and $\boldsymbol{v} = (v_1, v_2, \ldots, v_n)^T$. This leads to the following finite difference scheme:

$$\begin{pmatrix} \dot{\mathbf{u}} \\ \dot{\mathbf{v}} \end{pmatrix} = \begin{pmatrix} \boldsymbol{D}_{xx} & 0 \\ 0 & d\boldsymbol{D}_{xx} \end{pmatrix} \begin{pmatrix} \mathbf{u} \\ \mathbf{v} \end{pmatrix} + \begin{pmatrix} \mathbf{f}(u, v, p) \\ \mathbf{g}(u, v, p) \end{pmatrix}.$$

Considering a domain $\Omega = [-30, 30]$, we have a $2n \times 2n$ ODE system. We can utilise MATLAB's built-in time stepping ODE solvers, such as 'ODE15s', to generate numerical solutions. This approach allows us to obtain numerical evidence for the Hopf bifurcation at p_1^s and the Turing bifurcation at p_2^s. We initialise the system with small perturbations using the following initial condition:

$$(\boldsymbol{u}, , \boldsymbol{v})^T = \boldsymbol{u}^* + 0.01(\sin\frac{2\pi}{10}\boldsymbol{x}\,, \sin\frac{2\pi}{20}\boldsymbol{x})^T. \tag{6.2}$$

where $\boldsymbol{u}^*$ represents the steady-state solution and $\boldsymbol{x}$ the discretise domain.

By running the time stepping functions for a specified time t, we can plot the results using 3D plot functions. Figures [6.2] and [6.3] show the numerical results that correspond to the analytical solutions for the Hopf and Turing bifurcations, respectively.

Figure [6.4] demonstrates that after a significant amount of time, the solution for both u and v becomes periodically stable, as indicated by the wave pattern along the time axis. Additionally, it is interesting to note that since p_2^s was close to a Turing bifurcation point, the initial perturbation not only exhibits time oscillations but also spatial oscillations, as seen in the peaks of the solution for $t = [0, 15]$.

Similarly, Figure [6.5] shows the numerical analysis of the Turing bifurcation point p_3^s, where it is evident that the solution forms a spatial pattern consisting of three uniform peaks after a short time period. This provides numerical evidence that p_3^s corresponds to a Turing bifurcation.

6.2.2. Continuation

In the previous section, we presented a numerical method for classifying a bifurcation point, although we already had analytical information about the system. Now, we will introduce a

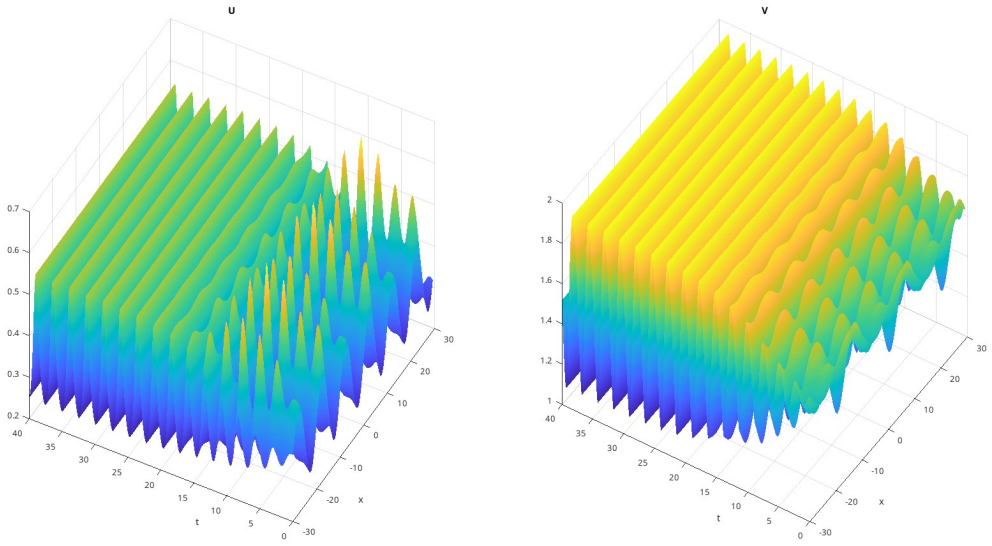

Figure 6.4.: Time stepping and 3D plot of the Hopf bifurcation point $p_2^s = (7, 0.15, 0.21, 20)$. The numerical results confirm that this point is indeed a Hopf bifurcation, as evidenced by the periodic pattern observed in the time axis.

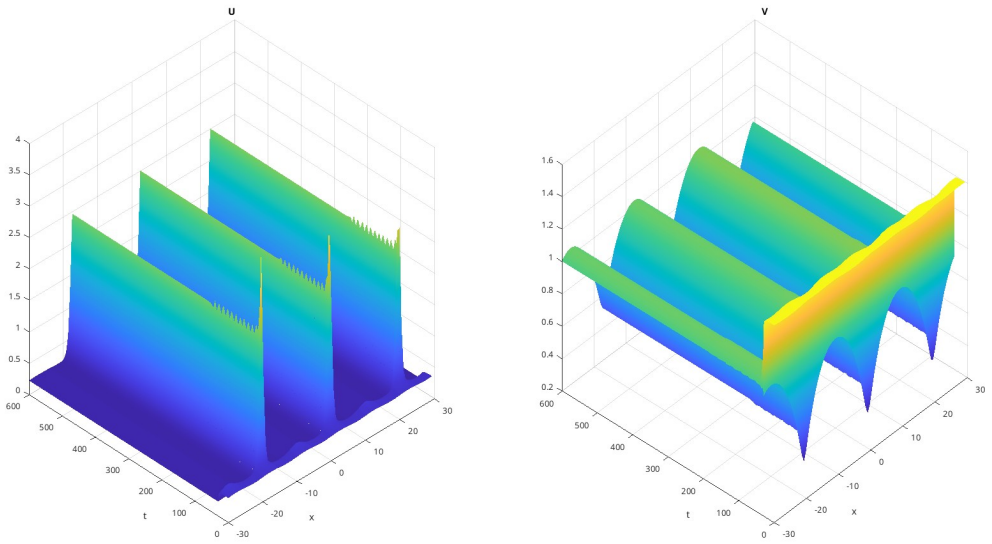

Figure 6.5.: Time stepping of the Turing bifurcation point $p_3^s = (7, 0.175, 0.21, 100)$. The periodic patterns observed in the spatial domain confirm that this point corresponds to a Turing bifurcation.

numerical method based on the continuation method to determine the location of bifurcation points in the parameter space and also provide a classification for the type of bifurcation.

Hopf Bifurcation

Consider $\boldsymbol{p} = (7, 0.15, b, 20)$. From Figure [6.2], we know that $b^* \approx 0.188$, indicating that for $b < b^*$, the steady state $\boldsymbol{u}^*$ is stable to small perturbations, while for $b > b$, the system undergoes a Hopf bifurcation. To provide numerical evidence for this claim, we utilise we implement in Matlab a continuation function with the parameters specified in Table 6.1. The continuation process begins with $b_0 = 0.16$ and iterates until either $b_i = 0.20$ or after 2000

Function parameters	values assigned
pMin	0.16
pMax	0.20
s0	0.1
sMin	0.00001
sMax	0.001
max Steps	2000

Table 6.1.: Parameter values for the continuation function.

Steps	$\lambda > 0$	b	u	v
249	0	0.1888636	0.33886	1.6447
250	0	0.1889342	0.33893	1.6447
251	2	0.1890047	0.33900	1.6446
252	2	0.1890751	0.33908	1.6445

Table 6.2.: Extract from the continuation function indicating the detection of a Hopf bifurcation point between steps 250 and 251.

steps. The initial step size is set to $s = 0.1$, and its value changes dynamically during the function execution, ranging between $s = [0.00001, 0.001]$. Table 6.2 shows a subset of the output from the continuation function at selected steps. At step 250, the system is stable, but at step 251, two eigenvalues cross zero. According to Theorem 2.5, this implies that the system becomes unstable. Figure [6.6] provides a visual representation of the numerical continuation from $b = 0.16$ to $b = 0.2$. The plot colour-codes the stability of the system, with blue indicating stability and red indicating instability. The colours also represent the number of eigenvalues with real parts above the $y = 0$ line. However, this information alone does not determine the specific type of bifurcation point. To gain further insight, we plot the spectrum of all the eigenvalues of the discrete system, as shown in Figure [6.7]. The plot indicates the presence of a pair of complex eigenvalues with zero real parts crossing the zero axis, suggesting a Hopf bifurcation or a Turing-Hopf bifurcation. To determine the nature of the bifurcation, we find the index j of the $\lambda_j > 0$ eigenvalues and plot their associated eigenvectors in Figure [6.8]. Several observations can be made: firstly, there is no periodic structure in the curve, and secondly, the amplitude of the y-axis is relatively small. The absence of periodicity confirms that the point corresponds to a Hopf bifurcation, which aligns with our initial analytical findings.

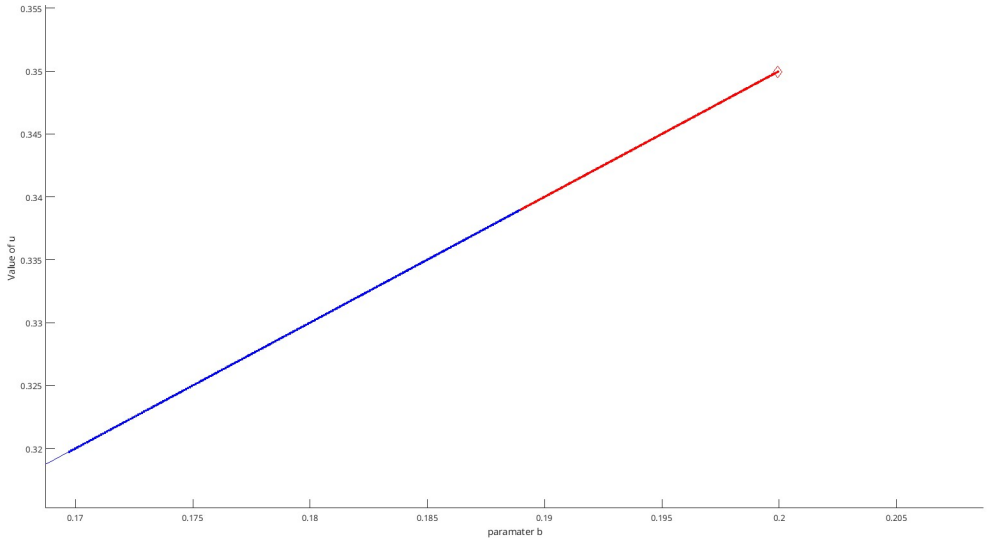

Figure 6.6.: Numerical continuation from $b = 0.16$ to $b = 0.2$. The system is stable when shown in blue and unstable when shown in red. The colours indicate the number of eigenvalues with real parts above $y = 0$.

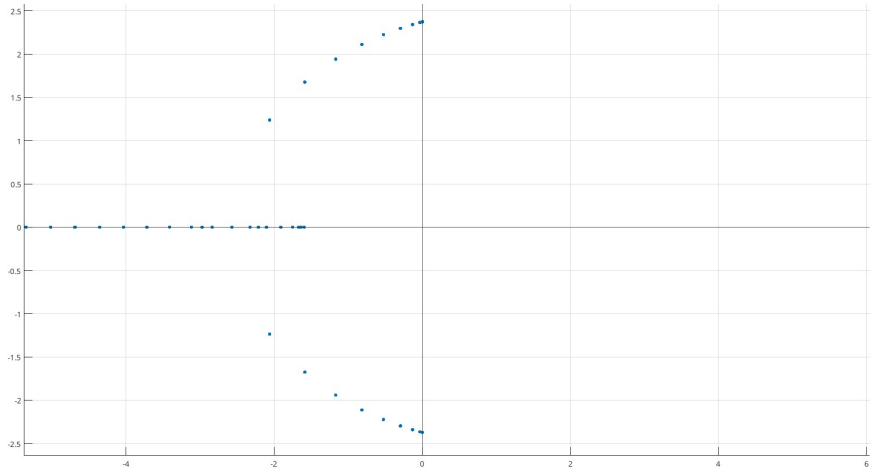

Figure 6.7.: Spectrum plot of the discrete matrix.

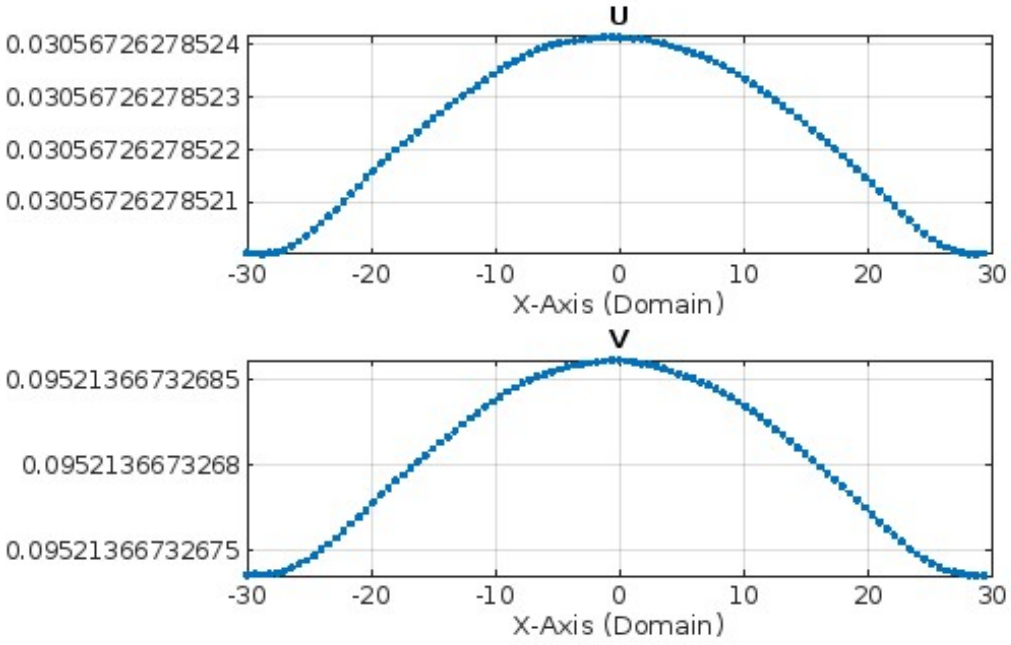

Figure 6.8.: Eigenvectors associated with $\lambda_j > 0$ for the Hopf bifurcation.

Steps	$\lambda > 0$	b	u	v
48	0	2.041586	0.37916	1.4201
49	0	2.042465	0.37925	1.4201
50	2	2.043342	0.37933	1.4200
51	2	2.044219	0.37942	1.4200

Table 6.3.: Extract from continuation function, detecting a Turing Bifurcation point.

6.2.3. Turing Bifurcation

Using the methods described in the previous section, we now set $\boldsymbol{p} = (7, 0.175, b, 100)$ and run the continuation function with the values specified in Table 6.1, this time changing b. Table 6.3 shows the relevant output steps, and at step 50, two eigenvalues become greater than zero, indicating a bifurcation point at $2.042465 < b^* \leq 3.043342$. Figure [6.10] presents the spectrum plot of the discrete matrix, showing that the imaginary part of the crossing eigenvalue is zero. According to Lemma 4.2, this indicates a Turing bifurcation. Additionally, Figure [6.11] displays the absolute values of the eigenvectors associated with the eigenvalue $\lambda_j > 0$. In contrast to the Hopf bifurcation, the Turing bifurcation exhibits a periodic structure with a relatively significant amplitude. This confirms the validity of our numerical analysis methods, as they align with the results obtained from the analytical analysis.

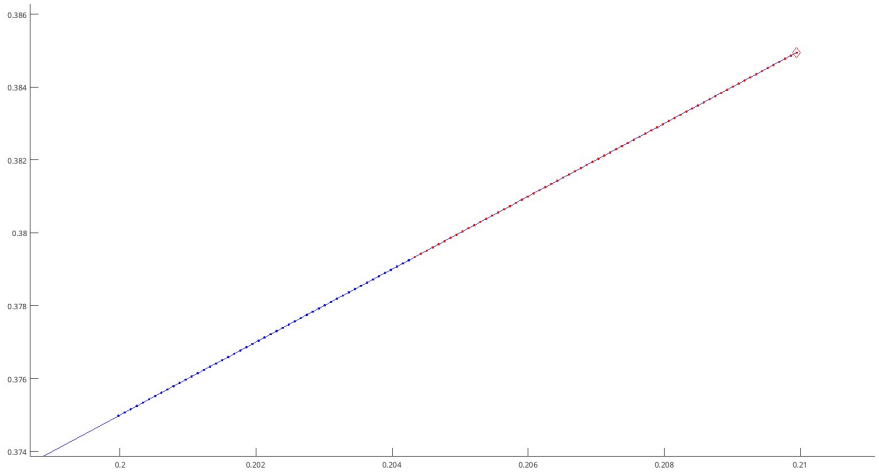

Figure 6.9.: Numerical continuation from $b = 0.19$ to $b = 0.21$. The system is stable when shown in blue and unstable when shown in red. The colours indicate the number of eigenvalues with real parts above $y = 0$.

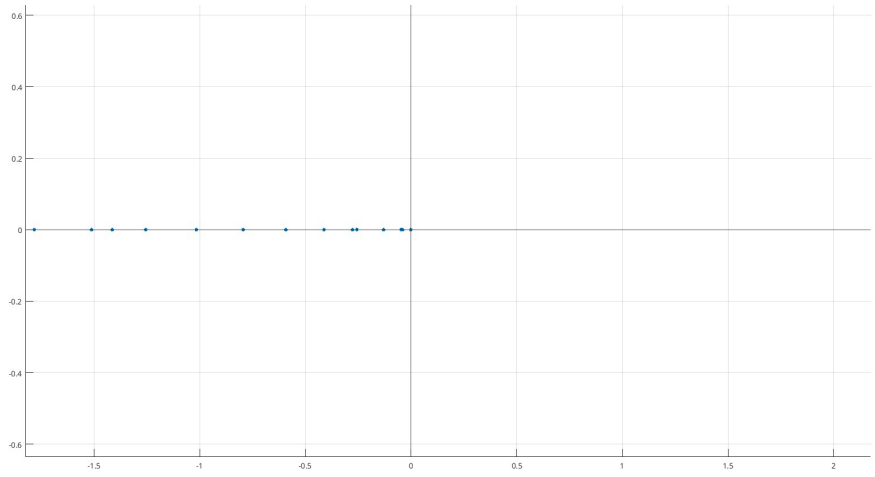

Figure 6.10.: Spectrum plot of the discrete matrix.

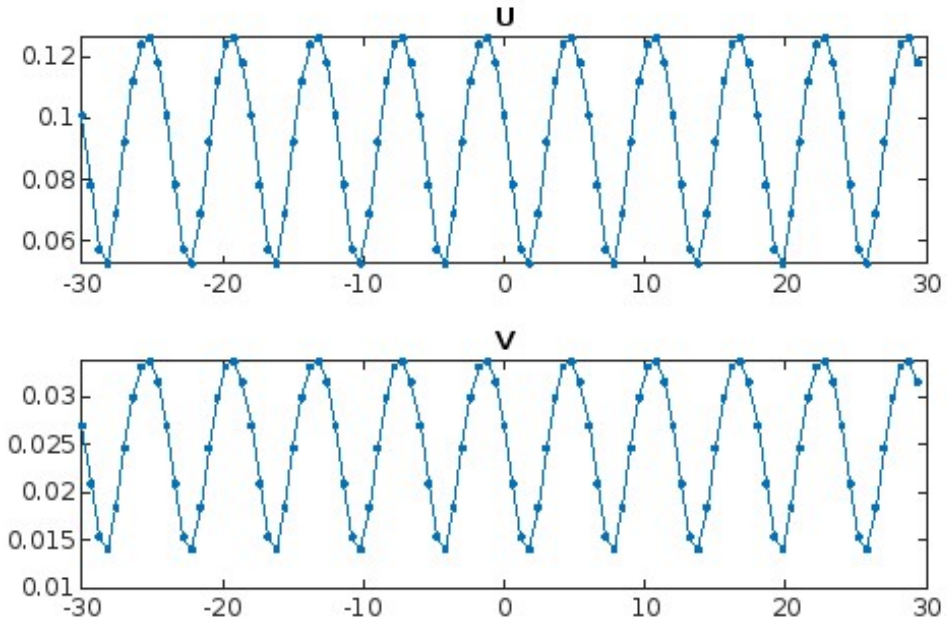

Figure 6.11.: Eigenvectors associated with $\lambda_j > 0$ for the Turing bifurcation.

7. Travelling Waves

This chapter provides an introduction to the fundamental concepts of wavetrains, which are also referred to as travelling waves. Wavetrains are solutions to partial differential equations that propagate at a constant wave speed c while maintaining their shape, including both wavelength and amplitude [10]. They can arise from Hopf bifurcation points, including Turing-Hopf bifurcation points. Travelling waves have been observed in various contexts, as documented in [13, 4].

The solution of a partial differential equation is denoted as $u(x,t)$, where x and t represent the spatial and time variables, respectively. We can express the solution in terms of the variable $\xi = x - ct$, which leads to $v(x-ct) = v(\xi) = u(x,t)$. A standing wave, characterised by $c = 0$, does not propagate and remains stationary.

There are different forms of travelling waves, but in this paper, we primarily focus on wavetrains. Wavetrains are spatially periodic waves, meaning that $v(\xi + \tau) = v(\xi)$ for all ξ and $\tau > 0$.

Stability analysis of travelling waves involves investigating whether a solution remains in the vicinity of the set of all translations of the travelling wave $v(\cdot)$ for all possible t. If this condition is satisfied, we say that the travelling wave is stable. On the other hand, if there exist initial conditions arbitrarily close to the wave such that the associated solution moves away from a small neighbourhood of the wave and its translations, the wave is considered unstable.

7.1. Reaction-Diffusion System

To illustrate the framework, let us consider the reaction-diffusion equations given by Eq. 3.1. By introducing the moving frame $\xi = x - ct$, we can rewrite the equation as follows:

$$u_t = Du_{\xi\xi} + cu_\xi = R(u). \tag{7.1}$$

Assuming that $u(\xi, t) = v(\xi)$ is a stationary solution of Eq. 7.1, we obtain:

$$Dv_{\xi\xi} + cv_\xi + R(v(\xi)) = 0. \tag{7.2}$$

This allows us to establish the associated eigenvalue problem by linearising Eq. 7.1 around the point $v(\xi)$, resulting in:

$$Du_{\xi\xi} + cu_\xi + \partial_u R(v)u =: \mathcal{L}u. \tag{7.3}$$

It is worth mentioning that Eq. 7.3 can be discretised and implemented into a continuation function, as mentioned previously. This enables us to analyse the stability of travelling wave solutions to reaction-diffusion equations using time-stepping methods.

8. Cellular Cytokinesis Model

The system of reaction-diffusion equations that is used to model the cortical patterns displyed on oocytes under specific parameters can be generalised from Eq.(1.1) to

$$\partial_t \mathbf{z} = \mathbf{D} \cdot \mathbf{z} + \mathbf{R}(\mathbf{z}, \mathbf{p}) \tag{8.1}$$

with the corresponding reaction function, and diffusion coefficients give as

$$\mathbf{z} = \begin{pmatrix} u \\ v \\ w \end{pmatrix}, \quad \mathbf{D} = \begin{pmatrix} d_u & 0 & 0 \\ 0 & d_v & 0 \\ 0 & 0 & d_w \end{pmatrix}, \quad \mathbf{R}(\cdot) = \begin{pmatrix} R(u, v, f(\alpha, \beta)) \\ R(u, v, f(\alpha, \beta)) - k_5 - k_6 v \\ k_7 + k_8 \frac{u^2}{1+k_9 u^2} - k_{10} w \end{pmatrix}.$$

while defining the parameter vector as

$$\boldsymbol{p} := (k_0,\, k_1,\, \ldots\, k_{10},\, \alpha,\, \beta,\, d_u,\, d_v,\, d_w)\,. \tag{8.2}$$

The anticipated behaviour of the model, concerning the model parameters α (Ect2) and β (RGA-3/4), is visually depicted in Figure [8.1]. The figure illustrates the regions of wave instability (blue) and oscillations (green), indicating the potential occurrence of waves. Specifically, zone 1 represents the higher homogeneous steady state (HSS), while zone 2 corresponds to the lower HSS. This bifurcation plot provides valuable insights into the model's response to variations in α and β, shedding light on the parameter regimes that lead to different dynamical behaviours. The figure serves as a comprehensive visualisation of the model's predicted behaviour, as outlined in [7].

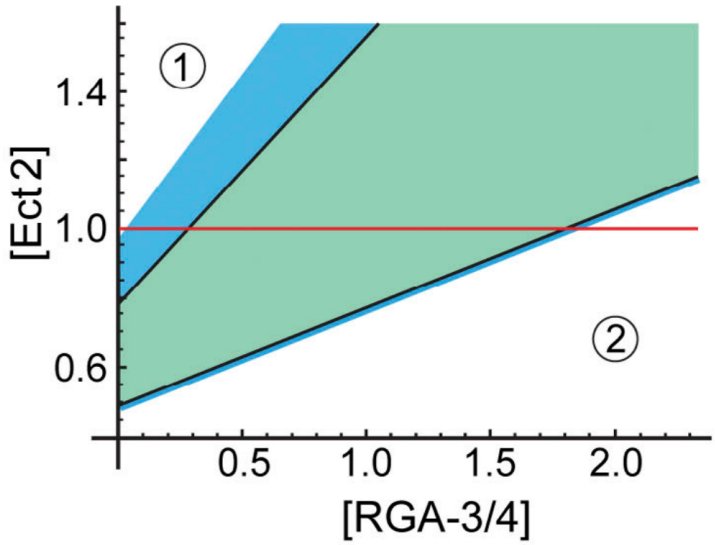

Figure 8.1.: Bifurcation plot depicting the behaviour of the system in relation to α and β parameters. The blue region represents wave instability, while the green region denotes oscillatory behaviour. Zone 1 corresponds to the higher HSS, and zone 2 represents the lower HSS. Adapted from [7].

Our objective is to perform a mathematical analysis of the model presented Eq.(8.1). By fixing $\alpha = 1$ and systematically varying the parameter β over a range of values, our main goal is to validate the predicted findings and investigate the presence of travelling waves within the model. Additionally, we aim to gain valuable insights into the stability properties of these waves under

specific conditions. Through a combination of analytical techniques and numerical simulations, we will thoroughly examine the model's dynamics, identify critical bifurcation points, and explore the existence and behaviour of travelling waves.

8.1. Numerical Results

Using the numerical methods mentioned in this paper, we conducted simulations to analyse the spatiotemporal dynamics of the reaction-diffusion model. Our findings reveal interesting bifurcation points and the emergence of travelling waves. We explored the parameter space of the model, specifically focusing on the β parameter in the range $[-0.3, 2.5]$. Through our numerical investigations, we identified two significant bifurcation points:

1. A Turing-Hopf bifurcation which occurs between $0.0370 < \beta^* < 0.0375$.
2. A Hopf bifurcation which occurs between $1.7626 < \beta^* < 1.7655$.

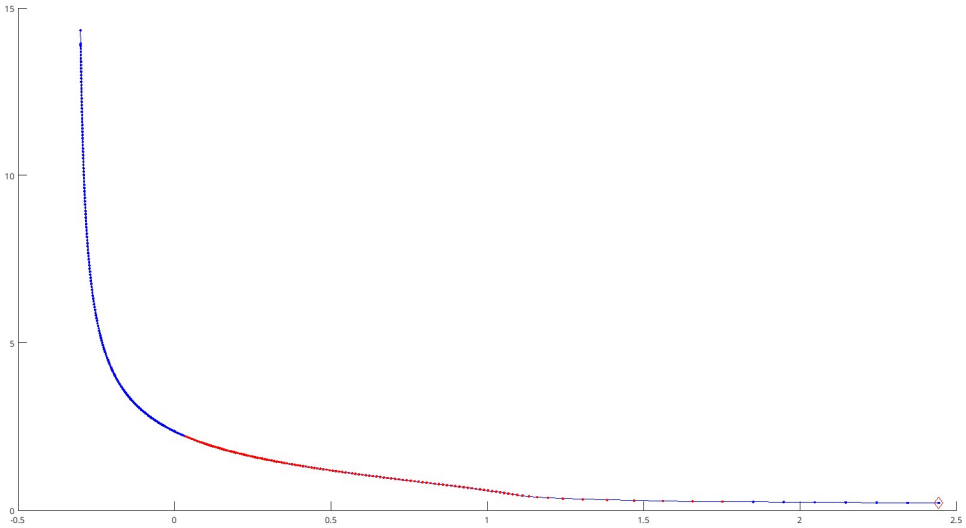

Figure 8.2.: Bifurcation diagram obtained via HSS continuous function for $\beta \in [-0.3, 2.5]$. With blue being stable states and red unstable. Note that the left side HSS is higher than the right HSS, corresponding to zones 1 and 2 in Figure [8.1]

Both bifurcation point are depicted in Figure [8.2], with the blue area of the curve visualising the stable solution and red the unstable. This matches the predicted behaviour of the system displayed in Figure [8.1]. Moreover, we discovered the presence of travelling waves in the system Figure [8.3], which are emitted due to the existence of the Turing-Hopf bifurcation point. Figure [8.4] illustrates the existence of a locus of travelling wave branches. By running numerous simulations, we tracked the behaviour of the main travelling wave branch. We observed the following stages:

i) The wave branch is unstable and transitions to a flat state for $\beta \in (3, 2.29)$.

ii) The wave branch becomes unstable, leading to changes in wave shape and speed around $\beta \approx 2.11$.

iii) A stable wave branch pattern emerges and persists for $\beta \in (-0.01, 1.95)$.

These results provide valuable insights into the spatiotemporal behaviour of the reaction-diffusion system and highlight the occurrence of bifurcations and travelling waves. The observed

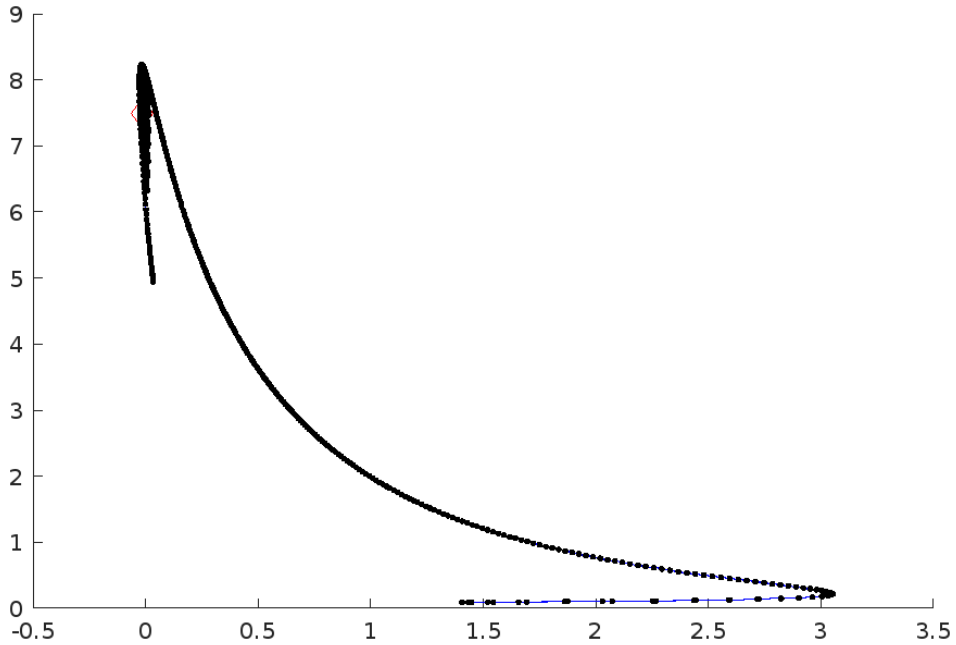

Figure 8.3.: Bifurcation diagram of the travelling wave, with y-axis the speed c and the x-axis β. Note that the left side begins for β of the Turing-Hopf bifurcation point.

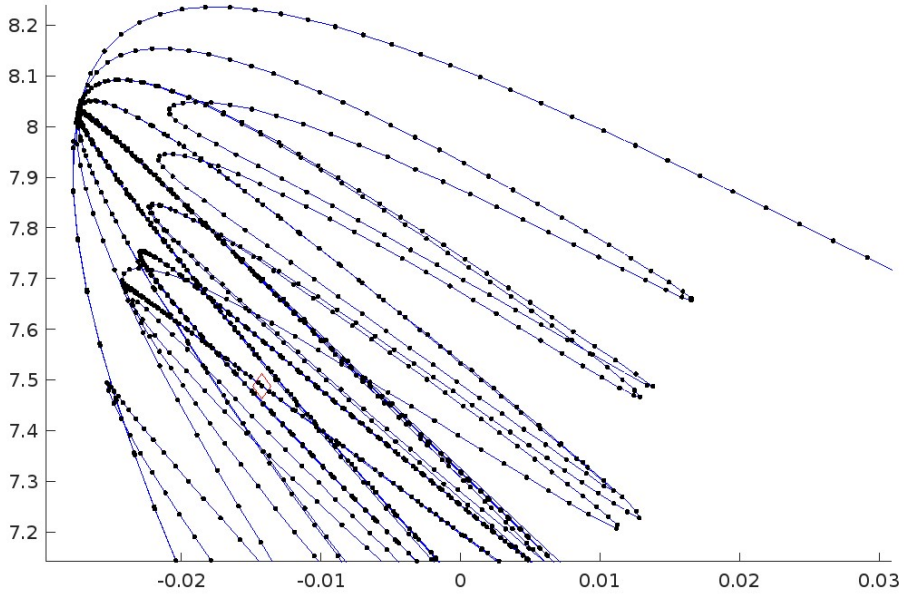

Figure 8.4.: A close up of the fold that occurs in the travelling wave bifurcation.

bifurcation points, including the Turing-Hopf and Hopf bifurcations, demonstrate the sensitivity of the system to changes in the β parameter. Additionally, the presence of travelling waves suggests the existence of self-organising patterns and dynamic behaviour in the model. These numerical findings contribute to our understanding of the underlying mechanisms driving the cortical excitability phenomenon and provide a basis for further exploration and analysis.

8.2. Methods

The application of numerical and simulation methods to analyse Eq. (8.1) is motivated by the complexity and lengthiness of the standard linear analysis. This becomes evident when formulating the dispersion relation using the eigenproblem:

$$\mathrm{Det}\left|\lambda \boldsymbol{I} - \mathbf{J} + k^2\mathbf{D}\right| = 0. \tag{8.3}$$

Here, the Jacobian for the system is defined as:

$$\mathbf{J} := \begin{pmatrix} -k_3 + v\left(-\frac{2k_1k_2u^4(1+\alpha)}{(1+k_2u^2)^2} + \frac{3k_1u^2(1+\alpha)}{1+k_2u^2}\right) - k_4w(1+\beta) & k_0 + \frac{k_1u^3(1+\alpha)}{1+k_2u^2} & -k_4u(1+\beta) \\ k_3 - v\left(-\frac{2k_1k_2u^4(1+\alpha)}{(1+k_2u^2)^2} + \frac{3k_1u^2(1+\alpha)}{1+k_2u^2}\right) + k_4w(1+\beta) & -k_0 - k_6 - \frac{k_1u^3(1+\alpha)}{1+k_2u^2} & k_4u(1+\beta) \\ -\frac{2k_8k_9u^3}{(1+k_9u^2)^2} + \frac{2k_8u}{1+k_9u^2} & 0 & -k_{10} \end{pmatrix}.$$

Consequently, this yields a characteristic polynomial of degree 3:

$$\lambda(k^2) := -\lambda^3 + \mathrm{Tr}(J)\lambda^2 - \frac{1}{2}\left[\mathrm{Tr}^2(J) - \mathrm{Tr}(J^2)\right] + \frac{1}{6}\left[\mathrm{Tr}^3(J) + 2\,\mathrm{Tr}(J^3) - 3\,\mathrm{Tr}(J)(J^2)\right]. \tag{8.4}$$

Computing the fixed point of the reaction-diffusion model, which involves 16 parameters, and subsequently analysing the dispersion relation curve for each fixed point, becomes a challenging task. Therefore, a more practical approach is to utilise numerical methods to transform the model into a linear system of ordinary differential equations.

8.2.1. Numerical bifurcation analysis

To approximate the model described by Eq. (8.1), we will utilise the Discrete method. We first choose an integer $n \in \mathbf{N}$ to represent the number of grid points for discretisation. Then, we define the vectors as:

$$\boldsymbol{u}(x,t) = (u_0, u_1, \dots u_n)^T, \quad \boldsymbol{v}(x,t) = (v_0, v_1, \dots v_n)^T, \quad \boldsymbol{w}(x,t) = (w_0, w_1, \dots w_n)^T. \tag{8.5}$$

This allows to approximate the reaction-diffusion system by a system of $3n \times 3n$ ODEs

$$\begin{pmatrix} \dot{\boldsymbol{u}} \\ \dot{\boldsymbol{v}} \\ \dot{\boldsymbol{w}} \end{pmatrix} = \begin{pmatrix} d_u\boldsymbol{D}_{xx} & 0 & 0 \\ 0 & d_v\boldsymbol{D}_{xx} & 0 \\ 0 & 0 & d_w\boldsymbol{D}_{xx} \end{pmatrix} \begin{pmatrix} \boldsymbol{u} \\ \boldsymbol{v} \\ \boldsymbol{w} \end{pmatrix} + \begin{pmatrix} \boldsymbol{f}(\boldsymbol{u},\boldsymbol{v},\boldsymbol{w},p) \\ \boldsymbol{g}(\boldsymbol{u},\boldsymbol{v},\boldsymbol{w},p) \\ \boldsymbol{h}(\boldsymbol{u},\boldsymbol{v},\boldsymbol{w},p) \end{pmatrix}. \tag{8.6}$$

Here, we set the domain of the model to $\Omega = [-50, 50]$ with $n = 199$ grid points. The parameter vector $\boldsymbol{p}$ is chosen as:

$$\begin{aligned} \boldsymbol{p} = \big(&0.0063, 0.1562, 1.0000,\ 0.0625,\ 0.0563,\ 0.0625,\ 0.0208, \\ &0.0019,\ 0.1406,\ 0.2500,\ 0.0250,\ 1.0000,\ \beta,\ 0.1600,\ 0.8000,\ 0.0002\big). \end{aligned}$$

To initialise the continuation function, we use the values specified in Table 8.1. We iterate over β from -1 to 2.5. Running the function produces Figure 8.2, and an excerpt of the results is displayed in Table 8.2. From the data, we observe that the system undergoes two bifurcation points: $0.0319 < \beta_1^* < 0.0368$ and $1.75 < \beta_2^* < 1.85$.

To analyse the two bifurcation points in more detail, we can increase the resolution of the continuation function. For the first bifurcation point that occurs around step 175, we adjust the parameters to $sMin = 1.0001$ and $sMax = 0.01$. We then run the continuation function at a higher resolution, resulting in the results shown in Table 8.3 and the continuation plot in Figure [8.5a]. To analyse type of β_1^*, we plot the spectrum of the complex pair of eigenvalues that become unstable in Figure[8.5b]. Additionally, we plot the absolute values of the associated eigenvectors in Figure [8.5c]. Based on this numerical evidence, it can be inferred that the bifurcation point at β_1^* is a Turing-Hopf bifurcation.

For the second bifurcation point β_2^*, which occurs around step 299, we follow a similar process. We adjust the parameters to $sMin = 0.0001$ and $sMax = 0.01$ and run the continuation function at a higher resolution. The results are depicted in Figure [8.5a], Figure [8.6b], and Figure [8.6c]. From this analysis, it can be concluded that β_2^* is a Hopf bifurcation point.

Function parameters	values assigned
pMin	-0.3
pMax	2.51
s0	0.01
sMin	0.00001
sMax	0.1
max Steps	2000

Table 8.1.: Parameters for the continuation function.

Steps	$\lambda > 0$	p	u	v	w
174	0	3.190335e-02	2.2210	3.0005	1.2500e+1
175	8	3.682844e-02	2.2016e+00	3.0005e+00	1.2402e+01
⋮	⋮	⋮	⋮	⋮	⋮
299	6	1.753578e+00	2.5816e-01	3.0005e+00	4.4372e-01
300	0	1.851038e+00	2.5040e-01	3.0005e+00	4.2224e-01

Table 8.2.: Extract of the results obtained for the low resolution continuation run.

Steps	$\lambda > 0$	p	u	v	w
588	0	3.370052e-02	2.2139	3.0005	1.2464e+01
589	4	3.375160e-02	2.2137	3.0005	1.2463e+01

Table 8.3.: Step 175, an extract from the continuous function output.

Steps	$\lambda > 0$	p	u	v	w
378	2	1.762614	2.5818e-01	3.0005	4.4470e-01
379	0	1.765539	2.5713e-01	3.0005	4.4086e-01

Table 8.4.: Step 299, results from the high resolution run.

8.2.2. Numerical travelling wave analysis

The presence of a Turing-Hopf bifurcation point β_1^* suggests the existence of a family of travelling waves that can emerge from this point. To explore this further, we employ the numerical continuation method. The continuation function is set up in a similar manner as before, with the same parameter details as in Table 8.1. By following the branch of the steady-state solution, we obtain Figure [8.3], where the y-axis represents the speed of the wave c and the x-axis represents the β parameter. Notably, the densely packed area of the curve is observed around the folding point at $\beta \approx 0.2$ and $c \approx 8$. To provide a more detailed view of this region, an enhanced plot is presented in Figure [8.4]. However, the continuation travelling wave function does not indicate whether a steady state is stable or unstable.

8.2.3. Time step simulations

To assess the stability of a steady state of a travelling wave, we employ a time step simulation of the linear system defined by Eq. (8.6). We extract parameter values and initial conditions from the travelling wave continuation function, which stores the steady state travelling wave profiles and their associated parameter values. By applying the time step function, we gain insight into

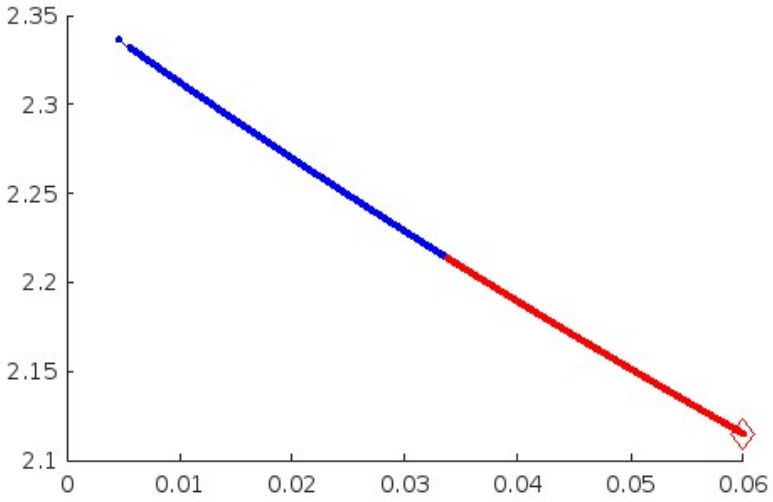

(a) Step 175, high resolution of the bifurcation diagram.

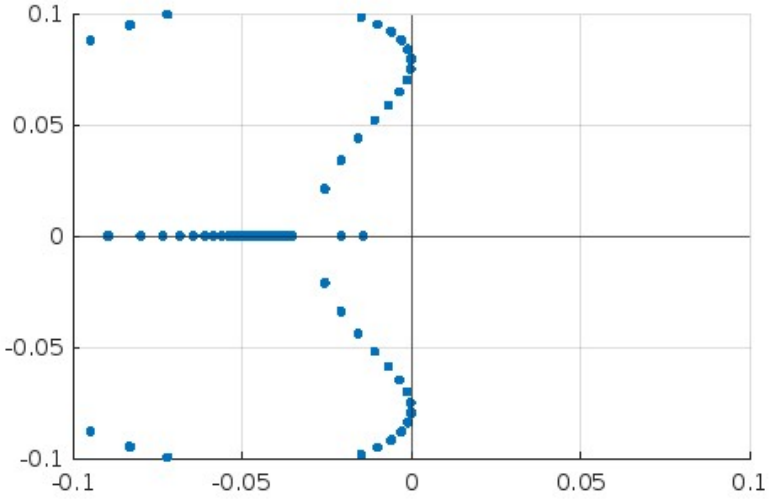

(b) Step 175 spectrum plot of eigenvalues.

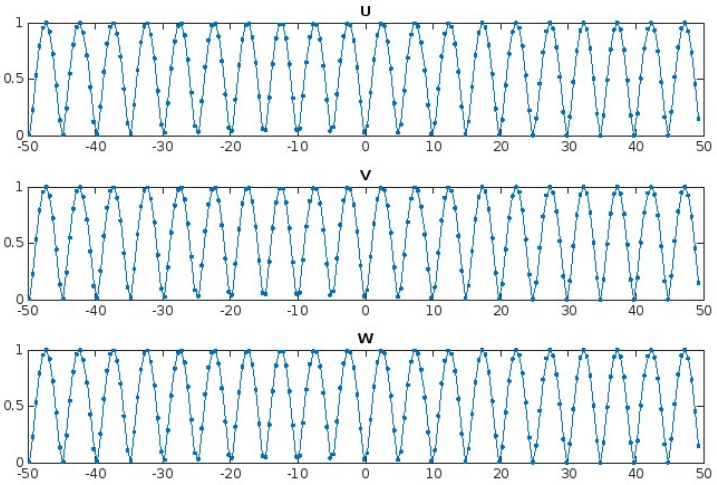

(c) Plot of the absolute values of the eigenfunctions of the associated unstable eigenvalues. Note the y-axis has been scaled, however the amplitudes are significant.

Figure 8.5.

the stability of the travelling wave over a specified time period.

The history of the time step function, presented as 3D plots, reveals the stability as time progresses. A stable travelling wave remains unchanged in shape and speed, while an unstable travelling wave undergoes variations in shape and/or speed. We repeat this process for a range of travelling wave points, allowing us to examine the behaviour of the model comprehensively.

Main branch

First, we conduct a series of time step simulations for the points along the "main branch," defined by the collection of points highlighted in Figure [8.7]. Through this analysis, we gather numerical evidence indicating that for $\beta \in (3, 2.29)$, the travelling waves are unstable and eventually converge to a flat homogeneous steady state. This dynamic is depicted in Figure A.1.

At $\beta \approx 2.11$, an interesting phenomenon occurs. The travelling wave is initially unstable but transforms into another travelling wave with a different shape and speed. This transformation is observed at iteration 130, as shown in Figure [A.2].

For the remaining range of $\beta \in (-0.01, 1.95)$, the travelling waves along the main branch are found to be stable. Figure [A.3] provides an example output of a time step simulation for one of these points.

Right-Hand-Side fold

For the iterations forming the branch defined in Figure [8.8], we observe that the travelling waves are unstable and eventually converge to the homogeneous steady state. However, at iteration 175 (Figure [A.4]), we notice an unusual pattern in the 3D plot. This pattern reveals mechanisms that have not been addressed in this paper and would require further investigation and research.

Left-Hand-side fold

Conducting a series of time step simulations along the Left-Hand-side of the main branch as shown in Figure [8.9], Our observations reveal that the waves are stable at the ends of this section, while they become unstable in the center. Interestingly, within this region of instability, as highlighted in Figure 8.4, we have observed the emission of multiple travelling waves branches.

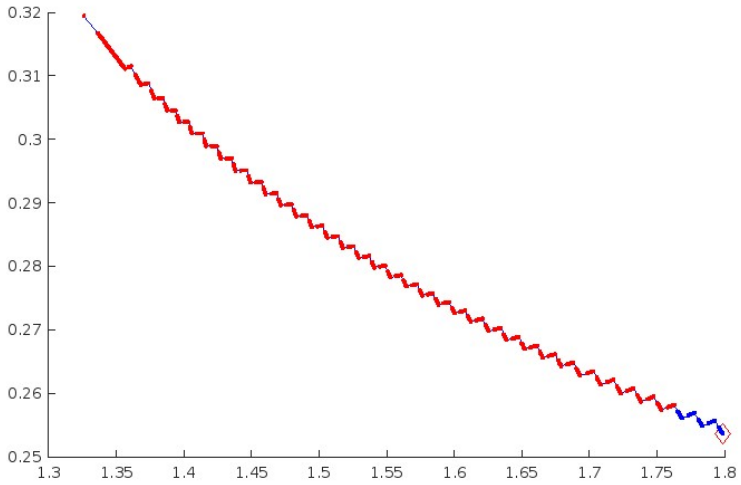

(a) Step 299, bifurcation diagram outputted from the high resolution run. The zigzag pattern is caused by approximation errors of steady states of the system while be computed.

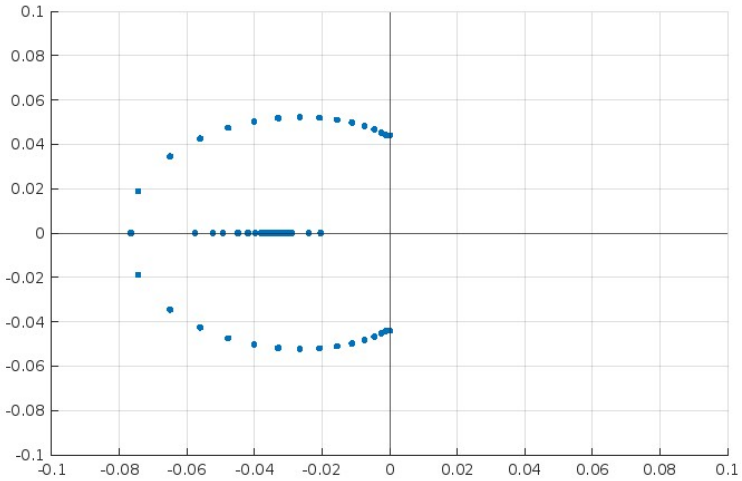

(b) Step 299 spectrum plot of eigenvalues.

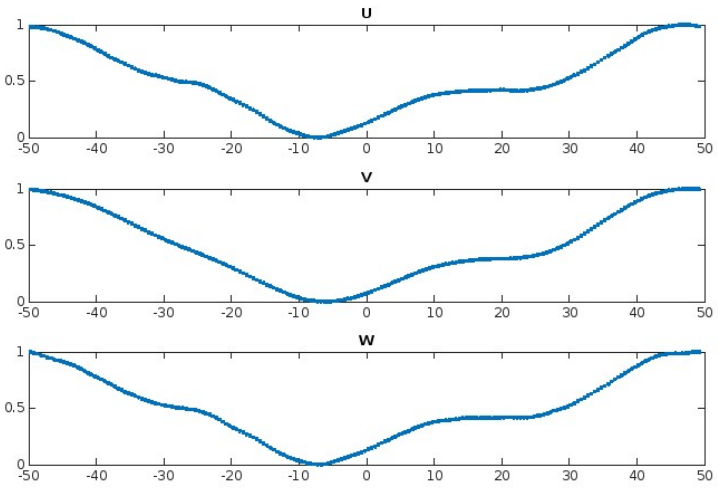

(c) Plot of the absolute values of the eigenvectors of the associated unstable eigenvalue. Note the y axis has been scaled, the amplitudes are insignificant.

Figure 8.6.

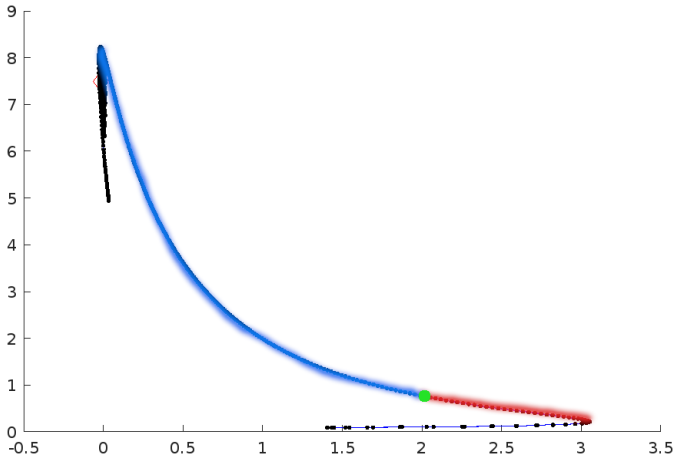

Figure 8.7.: A approximate guide to the main branch of travelling waves stability. Here blue represents stable and red is unstable. The green dot is for the wave branch becomes unstable, leading to changes in wave shape and speed, see Figure [A.2].

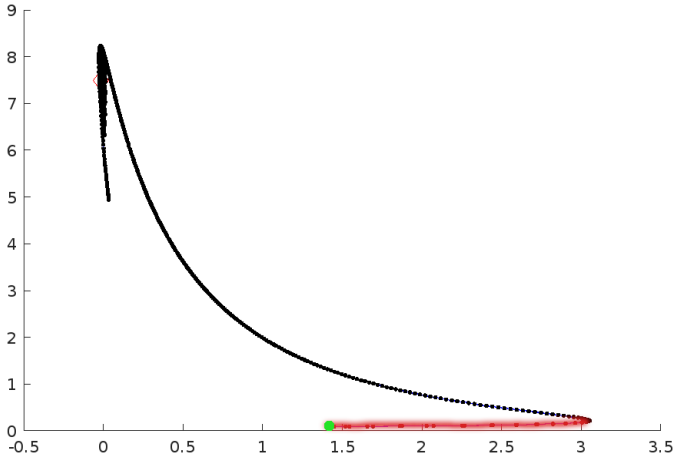

Figure 8.8.: The RHS fold branch off the main branch. The green dot is the pattern seen in Figure [A.4]

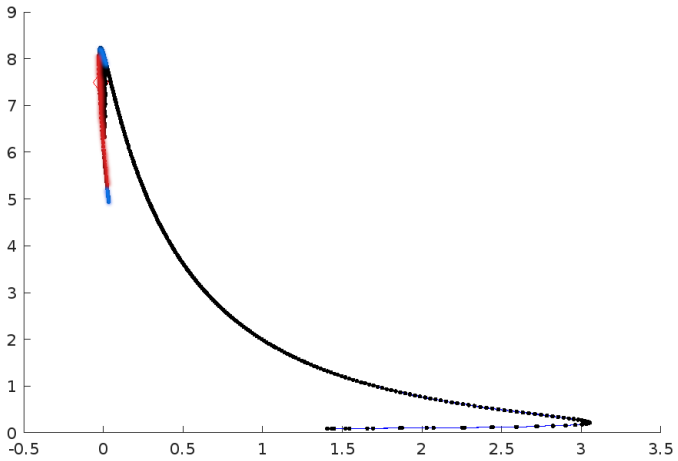

Figure 8.9.: The LSH of the main branch.

9. Conclusion

In this study, we have employed numerical methods, including discretisation, time stepping, and continuation, to investigate the spatiotemporal dynamics of a reaction-diffusion model Eq.(1.1) representing cortical excitability during cytokinesis. Our findings align with the results reported in [7] regarding the system's stability within the specified range of the β parameter.

Furthermore, we have successfully classified the two bifurcation points as Turing-Hopf and Hopf bifurcation points, leading to the discovery and analysis of a travelling wave within the predicted region of the bifurcation space. By exploring the parameter space and analysing the model's bifurcation diagram, we have identified critical points that mark qualitative changes in the system's dynamics.

Through multiple simulations, we have demonstrated the existence of travelling waves in the model system. We have tracked the behaviour of the main travelling wave branch, observing the stages of wave formation, stability, and transition. The stability of the travelling wave branch has been documented within specified ranges, and notable patterns have been identified, suggesting avenues for further research and investigation.

A. Time steps

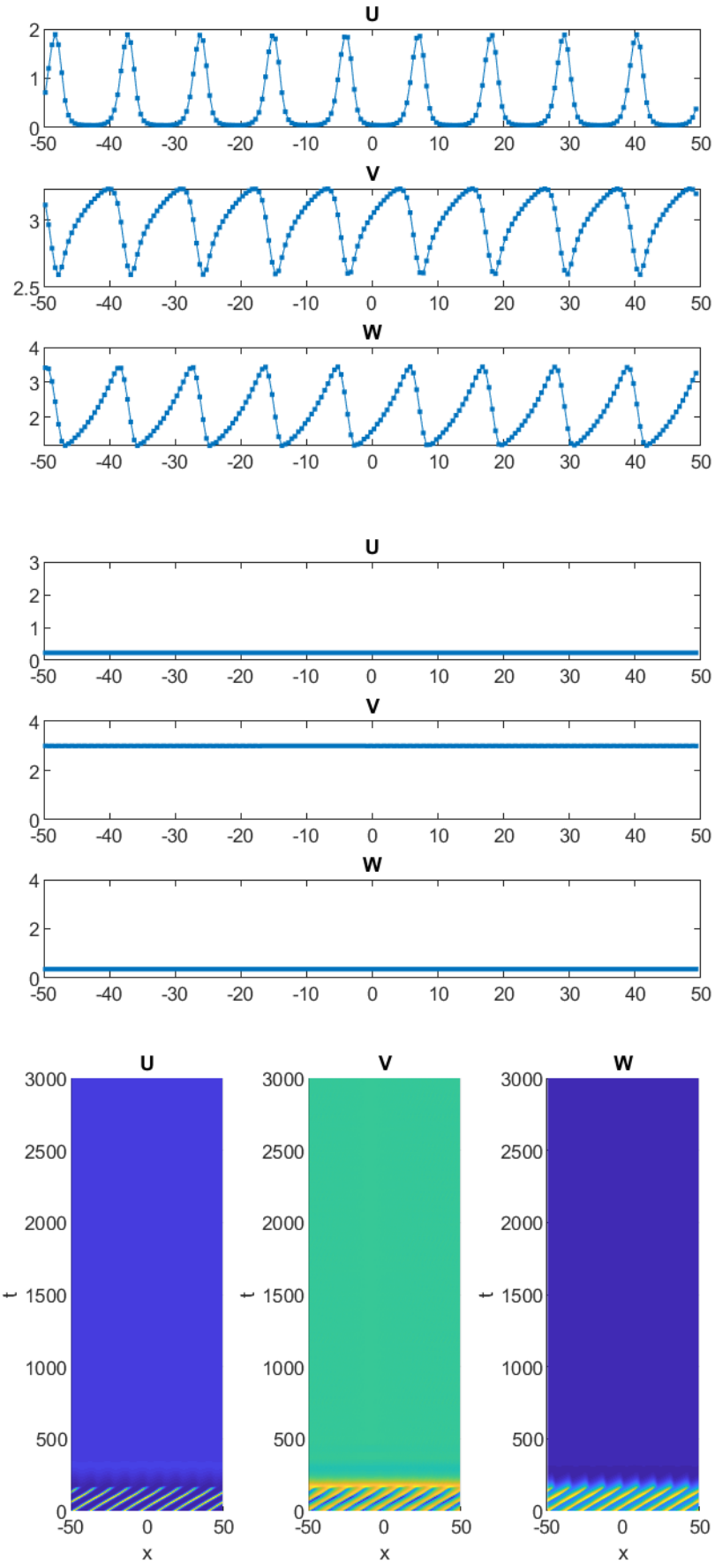

Figure A.1.: Iteration 135, $\beta = 2.2927$ and $c = 0.5952$

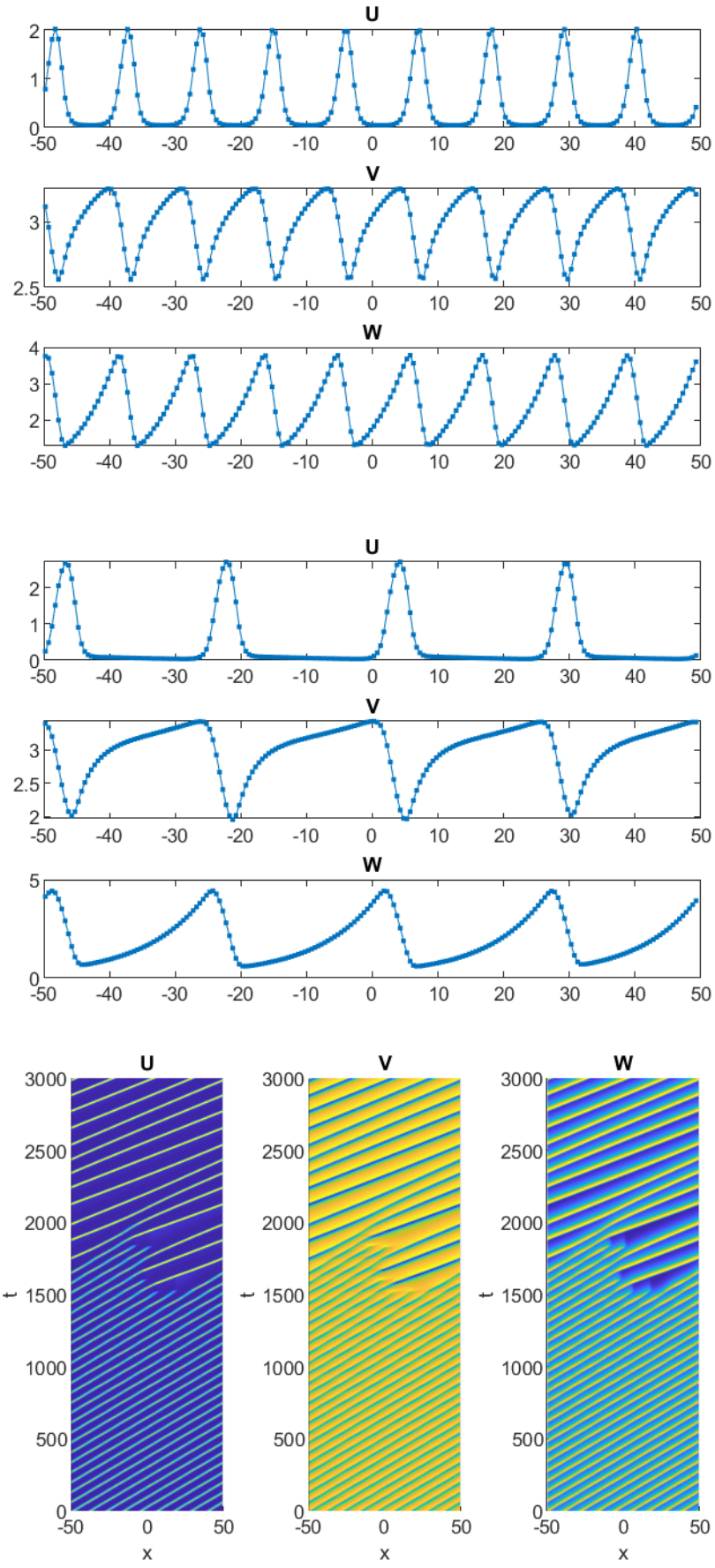

Figure A.2.: Iteration 130, $\beta = 2.1177$ and $c = 0.6947$

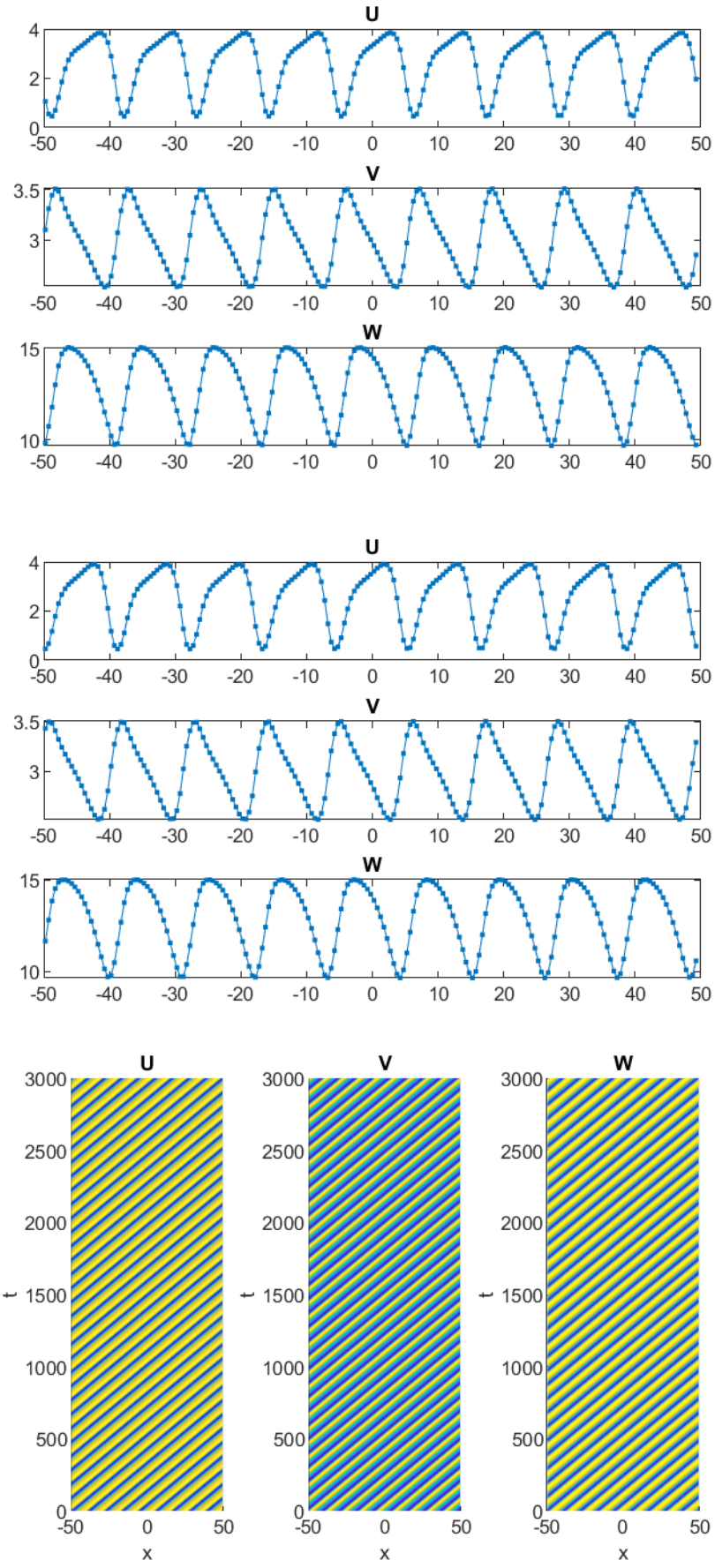

Figure A.3.: Iteration 447, $\beta = 0.0056$ and $c = 5.8856$. Note this the maximum speed observed.

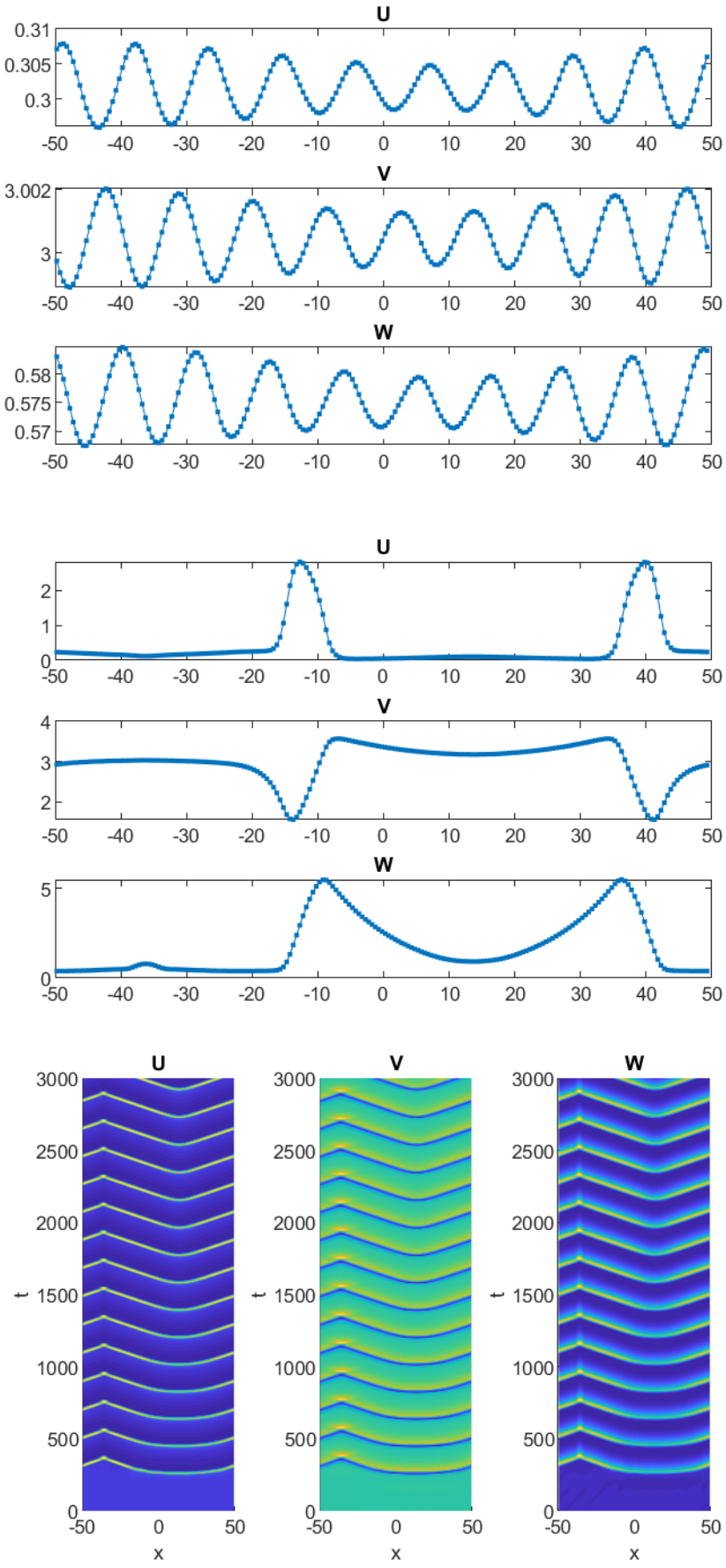

Figure A.4.: Iteration 175, $\beta = 1.4057$ and $c = 0.0919$.

Bibliography

[1] Mark Ainsworth, Jeremy Levesley, and Marco Marletta. *The Graduate Student's Guide to Numerical Analysis' 98: Lecture Notes from the VIII EPSRC Summer School in Numerical Analysis*, volume 26. Springer Science & Business Media, 2012.

[2] FRS Alan Turing. The chemical basis of morphogenesis. *Sciences-cecm. usp. br*, 1952.

[3] Rebecca B Hoyle. *Pattern formation: an introduction to methods*. Cambridge University Press, 2006.

[4] Christopher A Klausmeier. Regular and irregular patterns in semiarid vegetation. *Science*, 284(5421):1826–1828, 1999.

[5] Nancy Kopell and Louis N Howard. Plane wave solutions to reaction-diffusion equations. *Stud. Appl. Math*, 52(4):291–328, 1973.

[6] Bernd Krauskopf, Hinke M Osinga, and Jorge Galán-Vioque. *Numerical continuation methods for dynamical systems*, volume 2. Springer, 2007.

[7] Ani Michaud, Marcin Leda, Zachary T Swider, Songeun Kim, Jiaye He, Jennifer Landino, Jenna R Valley, Jan Huisken, Andrew B Goryachev, George von Dassow, et al. A versatile cortical pattern-forming circuit based on rho, f-actin, ect2, and rga-3/4. *Journal of Cell Biology*, 221(8), 2022.

[8] James D Murray. *Mathematical biology II: Spatial models and biomedical applications*, volume 3. Springer New York, 2001.

[9] Marc R Roussel. Reaction–diffusion equations. In *Nonlinear Dynamics: A hands-on introductory survey*. Morgan & Claypool Publishers, 2019.

[10] Björn Sandstede. Stability of travelling waves. In *Handbook of dynamical systems*, volume 2, pages 983–1055. Elsevier, 2002.

[11] J Schnakenberg. Simple chemical reaction systems with limit cycle behaviour. *Journal of theoretical biology*, 81(3):389–400, 1979.

[12] Guido Schneider and Hannes Uecker. Nonlinear pdes: A dynamical systems approach, volume 182 of. *Graduate Studies in Mathematics*, 2017.

[13] Jonathan A Sherratt and Gabriel J Lord. Nonlinear dynamics and pattern bifurcations in a model for vegetation stripes in semi-arid environments. *Theoretical population biology*, 71(1):1–11, 2007.

[14] S.H. Strogatz. *Nonlinear Dynamics and Chaos: With Applications to Physics, Biology, Chemistry, and Engineering*. CRC Press, 2018.

[15] Daniel Walgraef. *Spatio-temporal pattern formation: with examples from physics, chemistry, and materials science*. Springer Science & Business Media, 2012.